

## **HIGHLIGHTS.**

- Synthesis and characterization of a new naphthalimide-based PET sensor for pH sensing in aqueous media.
- The naphthalimide-based PET-sensor exhibits solvatochromic properties in organic solvents.
- The ensemble [CDs-naphthalimide-based PET sensor] shows a double functionality a) as H<sup>+</sup> sensor in aqueous media and b) as water sensing material in non-aqueous media (organic solvents and mineral oil-based lubricants).

# SMART CARBON DOTS AS CHEMOSENSOR FOR CONTROL OF WATER CONTAMINATION IN ORGANIC MEDIA.

Jorge Espina Casado, Alfonso Fernández-González, Marta E. Díaz-García, Rosana Badía-Laíño

Department of Physical and Analytical Chemistry, University of Oviedo, Oviedo, 33006, Spain.

## 1. ABSTRACT

A novel nanoprobe was synthesized by functionalizing glutathione/citric acid–carbon dots (CDs) with a benzo-isoquinolin-based molecule, methyl 3-(4-(2-(5-((methylsulfonyl)oxy)pentyl)-1,3-dioxo-2,3-dihydro-1H-benzo[de]isoquinolin-6-yl)piperazin-1-yl)propanoate (water chemosensor, WCS), to detect trace amounts of water in non-aqueous media via on-off fluorescence. The design and synthesis of the free molecule WCS and the functionalized nanoprobe (CD-WCS) are described in detail and as well as their full characterization by different spectroscopic methods. WCS was found to be an excellent indicator of pH in aqueous media and exhibited, in solvents of different polarity, solvatochromic behaviour. On the other hand, the modified fluorescence intensity of CD-WCS was found to be an excellent indicator for water in non-aqueous media (organic solvents and oil-based lubricants). In these media, CD-WCS showed weak fluorescence intensity due to a photoinduced electron transfer (PET) process. Sequential addition of trace amount of water led to revival of CD-WCS fluorescence intensity. The fluorescence on-off mechanisms are proposed for WCS in aqueous media as well as for CD-WCS in non-aqueous media. The analytical performance characteristics of CD-WCS showed a limit of detection for water of 0.00021% (v/v) in toluene and 0.00014 % v/v in base-oil lubricant. The potential application of CD-WCS as chemosensor of water contamination in oil-based lubricants as well as green anti-wear/anti-friction lubricant additive are outlined.

**KEYWORDS:** Carbon dots, chemosensor, water determination, organic solvents, lubricant oil

## 2. INTRODUCTION

Water in many organic solvents as well as in oily samples is generally considered as an impurity in a variety of industrial and technological sectors and it needs to be removed or determined in routine synthetic chemistry laboratories and in different industrial processes [1]. For example, a control of moisture in organic solvents must be performed as it destroys Grignard reagents, the most widely used reagents in organic and organometallic chemistry [2]. In a recent work by Meijer et al. [3] authors found that small amounts of water in methylcyclohexane destabilized of supramolecular polymers forming small aggregates. Also, solvents with very low water content must be used for sample preparation in GC as water may produce backflush during injection, a decrease in the efficiency of many stationary phases and interferes with some certain detectors such as flame ionization and electron-capture detectors [4]. The NMR spectral identification of solvents as impurities in synthesis and industrial processes may be interfered by the presence of water [5]. In the dry cleaning operations, the presence of water in the solvent used (e.g. perchloroethylene) must be carefully controlled so that the solvent relative humidity is the same as that which the delicate textiles would attain when in equilibrium with a room relative humidity at the same temperature of cleaning (usually not higher than 25°C) [6]. In the field of oil-based lubricants, moisture (water) contamination reduces its chemical stability and may cause many problems to machinery life such as corrosion, water etching (owing to by-products from lubricant degradation), vaporous cavitation (instantaneous vaporization and condensing implosion of water), hydrogen embrittlement (under extreme conditions water dissociates to release hydrogen atoms which then permeate the metal causing pinning and embrittlement of the metal) [7-9] among other effects.

Control of water contamination in lubricants and in organic solvents can be carried out by different approaches such as FTIR-chemometrics, photoacoustic spectroscopy, electrochemical impedance spectroscopy, coulometric Karl Fischer titration, different types of sensors (capacity, conductance, permittivity, viscosity), fiber optic devices, etc [10-14]. The determination of moisture/water in organic solvents using luminescent dyes has been addressed in different fluorescent formats, including immobilization of fluorescent dyes on a surface (glass, polymer, etc), metal-organic frameworks, photo-induced electron transfer (PET), intramolecular charge transfer (ICT) or europium-dye nanospheres [15-18].

Due to their unique physical and chemical properties, carbon dots are a versatile group of nanoparticles which have indeed attracted much attention and a systematic research started on their synthesis with different aims, such as luminescent nanoparticles for sensing and imaging, drug delivery, light emitting diodes, solar cells, etc [19-23]. In the last five years, carbon dots (CDs) have bursted into the development of novel sensing materials for water determination in organic solvents. Yan and Wu [24] developed a dual-emission chemosensor for moisture and water in organic solvents based on a green-Tb(III)-organic framework with red carbon dots. The probe worked as a ratiometric luminescent material within a relative humidity from 33.0% to 85.1% in the atmosphere. J. Wei et al [25] described the use of raw carbon dots as water-sensitive fluorescent probes in organic solvents such as ethanol, THF and 1,4-dioxane, with a detection limit of 0.01% v/v. Chao et al. [26] proved that CDs obtained by one-step hydrothermal treatment of o-phenylenediamine may act as visual sensors of the water content in organic solvents: emission gradually red shifted when the content of water increased, the color changing from cyan to orange to naked eye. Recently, Senthamizhan and co-workers [27] proposed different sensing mechanisms by which raw CDs may be sensitive to water in different aprotic and protic organic solvents. In aprotic solvents (THF, CAN and acetone) the red shift of the emission band of the CDs was used to monitor the water content, while in protic solvents (isopropyl alcohol and butyl alcohol) the fluorescence emission intensity was employed to determine the water content. Even, multifunctional CDs have been described that allowed not only trace water detection in organic solvents but also as fluorescent material for bioimaging and optoelectronic applications [28]. In this context, we present the synthesis of a PET dye (WCS) and its binding to glutathione/citric acid-based carbon dots with the aim to obtain a suitable fluorescent chemosensing material for monitoring water contamination in non-aqueous media. The behaviour of the WCS dye was studied in aqueous media and in both aprotic and protic solvents, observing a solvatochromic red shift of the fluorescence emission maximum upon increasing the polarity of the solvent. The binding of WCS to the surface of the glutathione/citric acid CDs (CDs-WCS) was characterized by different analytical techniques and it was found that the fluorescence intensity of the system increased as the water content in organic solvents and in oil lubricant increased. To our knowledge, this is the first time that fluorescent dye modified CDs have been adopted as water-sensitive probe in a complex sample such as a mineral lubricant oil as well as in an aprotic solvent (toluene). The signalling mechanisms of the luminescent probe have been outlined both in aqueous and non-aqueous media. There was an excellent agreement between the results obtained using

the CDs-WCS chemosensor and those obtained using the conventional Karl-Fischer coulometric method. What is more, the CDs-WCS offers potential green anti-wear and anti-friction additive for lubricants due to the presence of the CDs in the ensemble.

### **3. MATERIAL AND METHODS**

#### **3.1. Materials and reagents**

Citric acid (CA), L-glutathione reduced (GSH), 4-bromo-1,8-naphthalic anhydride, 5-amino-1-pentanol, piperazine, sodium bicarbonate, potassium iodide, methyl-3-bromopropionate, magnesium sulphate, triethylamine, dimethylaminopyridine, mesyl chloride, methanol, hydrochloric acid, sodium hydroxide, phosphoric acid and boric acid were purchased from Merck. Ethanol, chloroform, 2-methoxyethanol, tetrahydrofuran (THF), dimethyl sulfoxide (DMSO), ethyl acetate, dichloromethane, pyridine and anhydrous toluene (20 ppm water) were acquired to Sigma. Unless otherwise stated, Milli-Q water (MQW) was used throughout the experimental. 3.5 KDa Membrane Dialysis Tubes were bought to Merck.

#### **3.2. Instrumentation**

<sup>1</sup>H-RMN spectra were taken in a Bruker AV600 600 MHz and 14.0T. An AV300 300 MHz and 7.0T spectrometer was used for <sup>13</sup>C-RMN analysis. HRMS was performed in a Thermo Scientific Neptune Plus Spectrometer. FTIR spectra were recorded in a Varian 670 spectrometer, using 4 cm<sup>-1</sup> at 2000 cm<sup>-1</sup> resolution and 32 scans per sample. XPS experiments were carried out in an SPECS spectrometer with a Mg-K<sub>α</sub> X-ray source, using for high resolution spectra 0.1 eV and 30 eV as step energy and pass energy, respectively and 1 eV and 90 eV for survey spectra. The photoluminescence spectra of molecules and CDs were recorded in aqueous solution with an Edinburgh Instruments FLSP-920 spectrofluorimeter. The solutions were prepared in such a concentration that the absorbance was kept below 0.1. Absolute quantum yields were obtained by detecting all sample fluorescence through the use of an integrating sphere module in an FS5 Spectrofluorometer (Edinburgh Instruments) and the calculations were carried out by the instrument's Flu Oracle software.

High Resolution–Transmission Electron Microscopy (HR-TEM) images were obtained using a Tecnai F30 (FEI) Electron Microscope. Nanoparticles were dispersed in MQW and a couple of drops were put onto a copper grid, letting them to dry. Images were processed using Confocal Uniovi ImageJ compilation [29].

Water content in anhydrous toluene, in lubricant base oils and in different mixtures water-toluene was measured using a Coulometric Karl-Fischer device equipped with a diaphragm generator electrode model 899 from Metrohm. The sample amount ranged from 1 to 5 g, depending on water content, and commercial *Hydranal* from Fischer was used as electrolyte. Measurements were taken in triplicate and results reported as the average.

### 3.3. Synthesis of 3-(4-(2-(5-hydroxypentyl)-1,3-dioxo-2,3-dihydro-1H-benzo[de]isoquinolin-6-yl)piperazin-1-yl)propanoic acid (Water ChemoSensor, WCS)

The synthesis of WCS was carried out following the general procedure described by K.H. Kim et al [30] but introducing significant modifications as stated below (Scheme 1a-d):

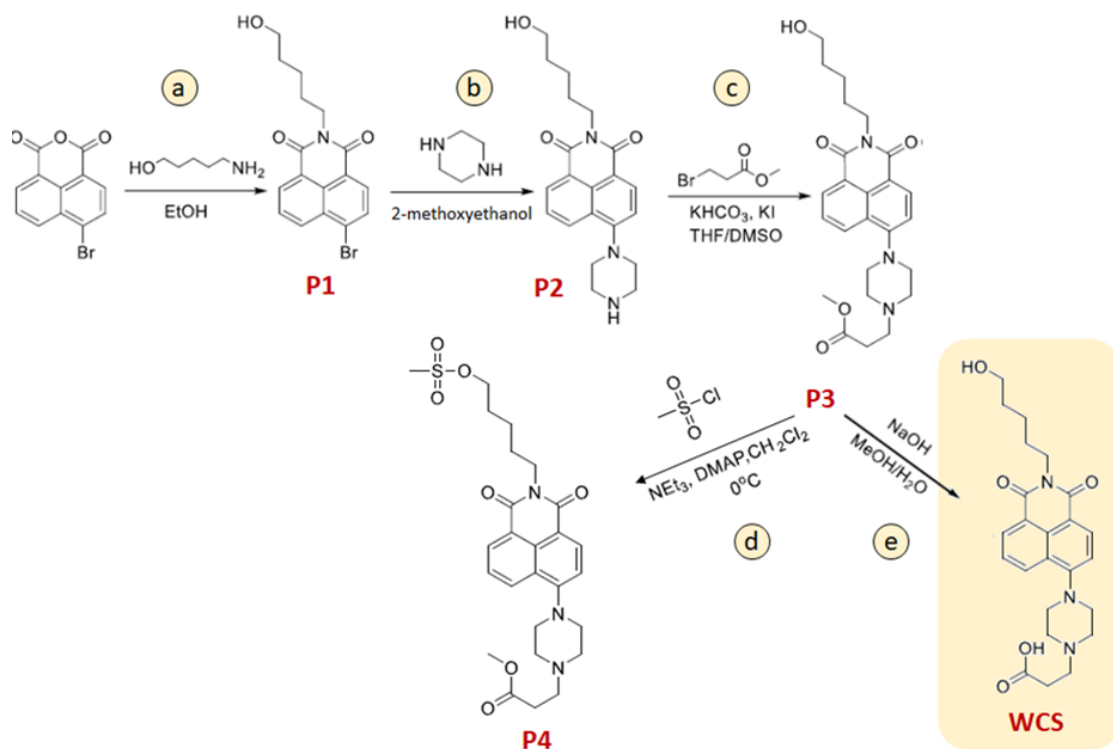
#### 3.3.a) Synthesis of 6-bromo-2-(5-hydroxypentyl)-1H-benzo[de]isoquinoline-1,3(2H)-dione (P1).

1.5 g (5.41 mmol) of 4-bromo-1,8-naphthalic anhydride and 670 mg (6.49 mmol) of 5-aminopentanol were dissolved into 30 mL of ethanol in a 100 mL flask. The mixture was heated under reflux at 85°C with constant stirring (300 rpm) for 9 h. Then, the mixture was let to cool down to room temperature and dried in a rotary evaporator-under reduced pressure. The solid was then dissolved in chloroform, filtered and evaporated to finally obtain 1.68 g (84% yield) of a yellow solid corresponding to the naphthalimide P1 (Scheme 1a). The product was characterized by <sup>1</sup>H-RMN (Figure S1a in Supplementary Information).

#### 3.3.b) Synthesis of 2-(5-hydroxypentyl)-6-(piperazin-1-yl)-1H-benzo[de]isoquinoline-1,3(2H)-dione (P2).

1.5 g (4.4 mmol) of P1 and 1.31 g (15.24 mmol) of piperazine were dissolved into 30 mL of 2-methoxyethanol. The mixture was heated under reflux at 140°C with constant stirring (300 rpm) for 2.5 h, after which it was let to cool at room temperature and the solvent was then removed under vacuum in a rotary evaporator. The reaction product was purified by recrystallization in ethanol. The product was dissolved in the minimum amount of hot ethanol and filtered while hot in order to remove possible traces of insoluble products. The

solution was finally let to stand and the resulting bright yellow crystals were collected using a Büchner funnel and washed with cold ethanol. 1.38 g of P2 crystals were obtained (Scheme 1b), that represented a 90% yield. P2 was also characterized with  $^1\text{H}$ -RMN (Figure S1b in Supplementary Information).



Scheme 1: Synthesis of P4 and WCS

3.3.c) *Synthesis of methyl 3-(4-(2-(5-hydroxypentyl)-1,3-dioxo-2,3-dihydro-1H-benzo[de]isoquinolin-6-yl)piperazin-1-yl)propanoate (P3).*

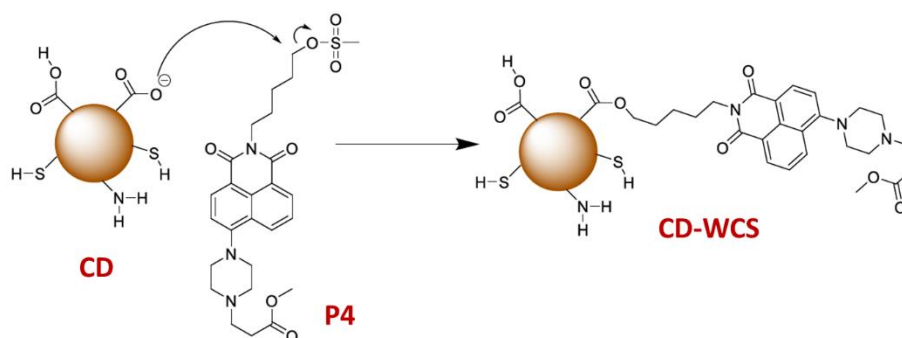
1.5 mg (4 mmol) of P2, 0.67 g (8 mmol) sodium bicarbonate and 330 mg (2 mmol) potassium iodide were weighed and dissolved into 30 mL THF plus 7 mL DMSO. Then, 675  $\mu\text{L}$  (6 mmol) of methyl-3-bromopropionate were added. The resulting solution was kept at 80°C under reflux for, at least, 48 hours. Then, the solution was let to cool at room temperature and 20 mL MQW were added. The reaction product was isolated by liquid-liquid extraction with (4  $\times$  20 mL) portions of ethyl acetate. The ethyl acetate solution was then washed with (4  $\times$  20 mL) portions of MQW and dried over magnesium sulphate (previously dried in an oven at 100°C). The solvent was evaporated under vacuum in a rotary evaporator to leave 1.34 g of a yellow solid (P3, Scheme 1c) with a yield of 72 %. P3 was characterized by  $^1\text{H}$ -RMN,  $^{13}\text{C}$ -RMN, HRMS (Figures S1c, S2a and S3a, respectively) and FTIR.

*3.3.d) Synthesis of methyl 3-(4-(2-(5-((methylsulfonyl)oxy)pentyl)-1,3-dioxo-2,3-dihydro-1H-benzo[de]isoquinolin-6-yl)piperazin-1-yl)propanoate (P4).*

0.5 g (1.1 mmol) of P3 were dissolved into 20 mL dry dichloromethane in a Schlenk flask under an inert atmosphere of N<sub>2</sub>. Then, 219  $\mu$ L (1.65 mmol) triethanolamine and 250 mg (1.5 mmol) dimethylaminopyridine were added under stirring. The flask was put into an ice-bath in order to cool it down to 0°C and then 500  $\mu$ L (6.6 mmol) mesyl chloride were slowly added to the mixture (Scheme 1d). The reaction was let to proceed at room temperature for 30 h after which it was neutralized via addition of 25 mL 0.1 M HCl. The solvent was vacuum removed in a rotary evaporator, obtaining 0.47 g of a highly viscous brown liquid (77% yield). The final product (P4) was characterized by <sup>1</sup>H-RMN, <sup>13</sup>C-RMN, HRMS (Figures S1d, S2b and S3b, respectively in Supplementary Information) and FTIR.

*3.3.e) Synthesis of 3-(4-(2-(5-hydroxypentyl)-1,3-dioxo-2,3-dihydro-1H-benzo[de]isoquinolin-6-yl)piperazin-1-yl)propanoic acid (WCS)*

0.25 g P3 (0.5 mmol) were dissolved in 5 mL methanol. Then 3 mL of an aqueous solution containing 0.144 g (3.12 mmol) NaOH were added. The mixture was left under constant stirring at 25 ° C for 4 hours, after which it was neutralized with 0.1 M HCl solution. The solvents were vacuum removed (rotary evaporator) and the product obtained was purified by preparative chromatography, using SiO<sub>2</sub> as stationary phase and a mixture chloroform:methanol 2:1 as mobile phase. 0.23 g WCS were finally obtained with a 95% yield. The final product was characterized by <sup>1</sup>H-RMN, <sup>13</sup>C-RMN, HRMS (Figures S1e, S2c and S3c, respectively in Supplementary Information) and FTIR.



Scheme 2: Synthesis of CD-WCS

### 3.4. Synthesis and functionalization of CDs (CD-WCS)

The synthesis of CDs was carried out via a hydrothermal process following the procedure described by T. Díaz-Faes et al. [31] with minor modifications. Briefly, in a porcelain crucible, 2 g of citric acid (10.4 mmol) and 1 g of reduced glutathione (3.2 mmol) were dissolved in 10 mL MQW. The crucible was introduced in an oven at 180°C for 2.5 h. At the same time, 1 mL water was added every 30 minutes by gently shaking the crucible in order to avoid the material to dry and its total pyrolysis. Once the hydrothermal process finished, the crucible was let to cool down to room temperature and the product obtained, an intense orange gel, was dissolved in 10 mL MQW. The solution, containing the CDs was dialyzed against MQW for 6 hours (×2), using 3.5 kDa membrane tubes. The dialyzed product was vacuum concentrated in a rotary-evaporator, until the final volume was reduced to the third of the initial volume. The final concentrated solution, brown-orange colour, was lyophilized to obtain 0.3 g of a fibrous brown solid of CDs, which was kept at 4°C until further use.

For the surface functionalization of CDs with P4, two different solutions were prepared: a first one with 0.4 g CDs dissolved in 2.5 mL pyridine and a second solution containing 0.11 g (0.2 mmol) P4 dissolved in 2.5 mL pyridine. Both solutions were then mixed in a flask and let to react at room temperature for 24 hours under constant stirring (360 rpm). Then, the solvent was vacuum removed and the dark orange solid obtained was dissolved in 5 mL MQW. The solution was centrifuged at 5200 rpm in order to eliminate any insoluble product and the supernatant liquid was dialyzed against MQW for 6 hours (×2), using 3.5 kDa membranes tubes. Once the solution was purified, the solvent was vacuum removed to the third of the initial volume. The concentrated solution was finally lyophilized yielding 0.09 g of a dark orange solid of CD-WCS (Scheme 2.1).

### **3.5. Influence of pH on the photoluminescence of WCS and CD-WCS**

Solutions of WCS ( $10^{-5}$  M) and CD-WCS (1 ppm) were prepared in a universal Britton-Robinson buffer and the desired pH between 2 and 12 was adjusted using the necessary amount of NaOH 0.4 M. The emission spectra of CD-WCS solutions at each pH were recorded by excitation at 345 nm and 395 nm, whereas that of WCS solutions were excited at 395 nm.

### **3.6. Water determination in commercial toluene and in lubricant base oil.**

Commercial toluene (CT) was used to prepare individual standard solutions of  $5 \times 10^{-4}$  M WCS, 50 ppm CD-WCS and 480 ppm water in toluene (water saturated toluene). From the last, by adequate dilution with CT, a 250 ppm water solution (Standard Water-Toluene Solution, SWTS) was prepared. The water content of SWTS was determined by coulometric Karl-Fischer titration. In 5 mL flasks, 100  $\mu$ L of the 50 ppm CD-WCS solution were added and dosed with the SWTS solution in concentrations of 0, 25, 75, 120 and 160 ppm water. Finally, each sample was diluted to final volume with CT. In the case of the lubricant base oil ISO-32, it was necessary to dilute the samples with CT in order to minimize the oil background fluorescence. Oil samples were diluted 0.1% v/v Oil/CT and analysed by standard additions following the same protocol as described for CT. All the glassware was vacuum dried for, at least, 24 hours prior to its use. All the solutions once prepared were kept, with paraffin-sealed stoppers, in desiccators until use. Water content in all solutions was also determined by coulometric Karl-Fischer titration.

## 4. RESULTS AND DISCUSSION

### 4.1. Synthesis and morphological/functional characterization of CD and CD-WCS

Schemes 1 and 2 show the different synthesis steps followed to obtain the water chemosensor molecule in its free form (WCS) and its linking to carbon quantum dots (CD-WCS). Both materials were obtained from P3. So, a simple alkaline hydrolysis in methanol-of the methyl ester P3 allowed getting the WCS molecule. However, in the case of linking the WCS molecule to CDs surface, it was necessary to prepare the P4 intermediate, which was then bound to the CDs surface. The CDs were obtained in a *bottom-up* approach by the widely-used hydrothermal method [32-34]. Two different carbon sources were used: citric acid and reduced glutathione, a tripeptide constituted by  $\gamma$ -Glu-Cys-Gly. Glutathione not only was a source of carbon, but also provided  $-\text{NH}_2$  and  $-\text{SH}$  functional groups to passivate the CDs surface and for further surface functionalization [35]. The ATR-FTIR spectrum of the obtained CDs (Figure 1) shows the presence of bands belonging to the functional groups present in the original glutathione, such as  $-\text{COOH}$ ,  $-\text{NH}_2$  and  $-\text{SH}$ , thus indicating their persistence upon the hydrothermal synthesis (see also Table S1 in Supplementary Information). There are also a broad and weak band around  $2530 \text{ cm}^{-1}$ , characteristic of the S-H stretching vibration of glutathione, another band around  $1696 \text{ cm}^{-1}$  attributable to stretching vibrations of carboxylic  $\text{C}=\text{O}$  and other one at  $1600 \text{ cm}^{-1}$ , assignable to in-phase

and out-of-phase stretching vibrations of the amide C=O group. The typical broad band of carboxylic acids (coming from citric acid) appears at  $3000\text{ cm}^{-1}$ , whereas a weak band, belonging to the stretching vibrations of N-H groups, appears between  $3400$  and  $3600\text{ cm}^{-1}$ . The bands are slightly shifted and/or broadened due to the local nano-environment of the CDs and/or the synthesis process, which may change the strength of some bonds.

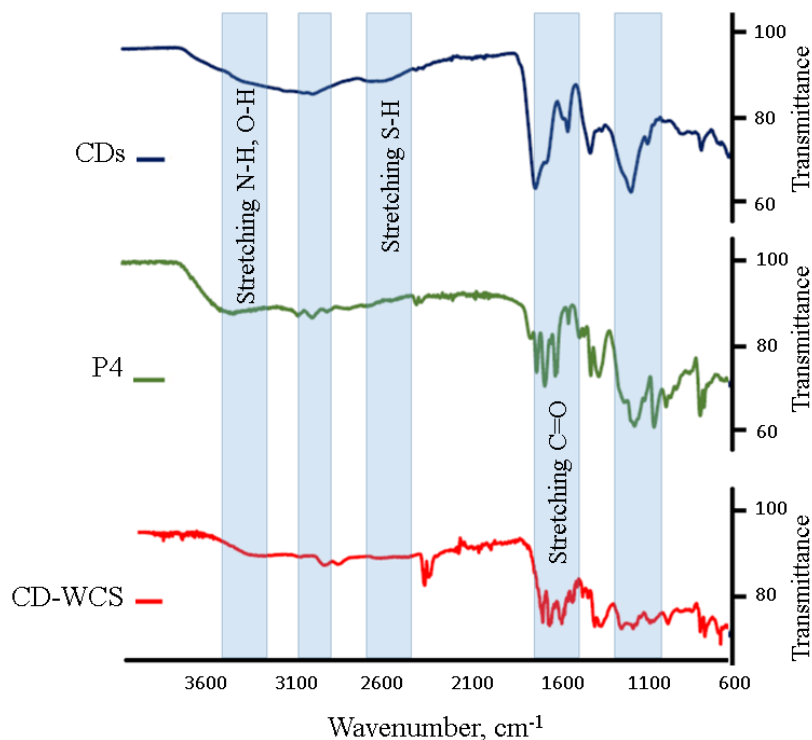


Figure 1. ATR-FTIR spectra of neat CDs, P4 and CD-WCS.

In order to confirm the presence of such functional groups on the CDs surface, the samples were analysed by XPS. The XPS spectrum, scanned from  $1200$  to  $1\text{ eV}$ , clearly exhibits the peaks corresponding to C1s ( $286\text{ eV}$ ), O1s ( $532\text{ eV}$ ), N1s ( $400\text{ eV}$ ) and S2p ( $160\text{ eV}$ ), with low intensities in the case of the latter two elements. Figure 2 shows the high resolution spectra of the four elements. C1s spectrum was fitted using four different type of carbon atoms, positioned: at  $284.2\text{ eV}$  (usually attributed to graphitic  $\text{sp}^2\text{ C=C}$  structure), at  $285.2\text{ eV}$  indicating the existence of C-O, C-S and/or C-N bonds, at  $286.6\text{ eV}$  belonging to C-S environment [36] and, finally, at  $288.4\text{ eV}$  assignable to C=O amide group [37, 38].

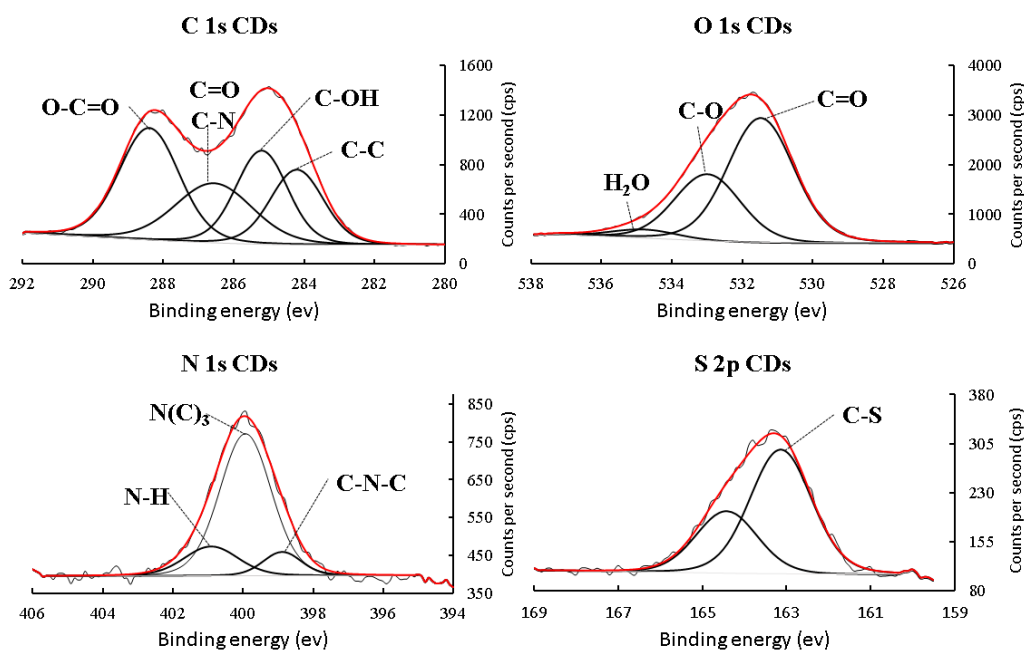


Figure 2. XPS High Resolution C1s, O1s, N1s and S2p spectra for CDs.

On the other hand, the N1s high resolution spectrum reveals the presence of three different components: a first one appearing at 398.9 eV, assignable to  $-N=$  [39], which points to a possible oxidation/deprotonation process of glutathione during the synthesis; a second major band at 399.9 eV assignable to  $NH_2$  [40], and a third one at 400.9 eV due to the single C – N bond in the amide moiety,  $NHC=O$  [41]. The presence of all these nitrogen bands is compatible with the existence of glutathione-related structures in the surface of the CDs. In the case of O1s, three components were also found. The most intense one appears at 531.5 eV and is assigned to C-O; the second one, with a medium intensity appears at 533 eV due to the C=O bond [42] and the third band, the weaker one, appears at 534.8 eV and may be related with adsorbed water in the solid. S2p spectra shows two components: the most relevant at 163.1 eV is related to C-S bond (with a formal oxidation state of -2) and other weaker at 164.3 eV assigned to species in higher oxidation degrees [43]. XPS was used to explore the semi-quantitative chemical composition of the surface of CDs following the C1s, N1s, O1s and S2p photoelectron spectra, resulting in 62% C, 29% O, 5% N and 4% S (atomic %). These composition and percentages data are in good agreement with the expected composition of the CDs, prepared from glutathione and citric acid [31].

P3 should be bound to the quantum dots surface through the hydroxyl group at the end of the C-5 chain as the  $-OH$  group in the propyl chain is esterified,  $-CO-O-Me$ . So, the C-5 hydroxyl group was activated through a bimolecular nucleophilic substitution ( $SN_2$ ) [44] with

a good leaving group as mesyl chloride (Scheme 1d) to obtain the intermediate P4. The reaction between P4 and CDs also proceeded through an SN2 reaction (Scheme 2), in which pyridine acted as an activator, speeding up the reaction, by mopping up any proton released from –COOH or -SH groups (present on the CDs surface) during the course of the reaction. These groups, along with –NH<sub>2</sub> also present on the CDs surface, may act as nucleophiles with loss of the mesyl leaving group and, in a concerted process, the CDs surface nucleophiles formed the corresponding bonds with P4, resulting in the CD-WCS (Scheme 2) formation.

The synthesis steps to obtain P4 were followed by <sup>1</sup>H-NMR and <sup>13</sup>C-NMR and the HRMS and ATR-FTIR spectra of each intermediate compound (see Supplementary Information) were recorded, whereas the CD-WCS system was characterized using TEM and FTIR. Figure 1 shows the ATR-FTIR spectra of CD-WCS (red line) and that of the two main substances involved in its synthesis. The CD-WCS spectrum shows some of the characteristic bands of the starting compounds (see Table S1). The stretching vibrations of O–H bonds from unreacted carboxylic groups and unreacted N–H bonds on the CD surface appear overlapped as a broad and weak band between 3200 and 3500 cm<sup>-1</sup>. Comparison of the same band present in the free CDs reveals that both the width and the intensity of the band have decreased, which is consistent with lower free functional groups due to their covalent reaction with P4. On the other hand, the band at 2600 cm<sup>-1</sup>, ascribed to the -SH groups, exhibits similar features in CD and CD-WCS spectra, which may be a proof that the reaction of P4 with CDs takes place preferably between carboxylic and amino groups. Additionally, the characteristic bands of P4 at 2932 cm<sup>-1</sup> and 2984 cm<sup>-1</sup>, are assigned to stretching vibrations of C with hybridization sp<sup>3</sup> and sp<sup>2</sup> while bands at 1684 cm<sup>-1</sup> and 1645 cm<sup>-1</sup> corresponding to stretching vibrations of C=O group are clearly seen also in the CD-WCS spectrum. A shoulder around 1700 cm<sup>-1</sup> from C=O of carboxylic groups [45] in CDs and CD-WCS is also detected. It is also interesting to observe that the FTIR spectrum of CD-WCS is closely similar to the combination of P4 + CDs spectra. In fact, the only difference between them is the absence in the CD-WCS spectrum of the intense P4 bands due to the sulphonate group at 1345 cm<sup>-1</sup> and 1199-1145 cm<sup>-1</sup> (asymmetric and symmetric vibrations of S=O, respectively). All these data confirm the proper functionalization of CD with P4. The HRTEM images (Figure S4) showed that both CDs and CD-WCS appear as spheres with a certain degree of crystal structure and a mean lattice parameter 0.24 nm. This value agrees with that of graphene [1 0 0] planes [46]. CDs and CD-WCS particle size

measurements were taken in a random particle selection of 264 items. Size histograms of both types of particles (Figure S5) showed a monodisperse Gaussian distribution, having the nanoparticles a diameter within the range of 2.5-3.0 nm. Therefore, functionalization did not affect significantly the dimensions of the carbon dots.

#### 4.2. UV-vis and luminescence spectroscopic characterization

The UV-vis absorption spectrum of neat CDs (Figure 3) shows an intense absorption band at 248 nm and a less intense one at 350 nm. The first band is attributed to  $\pi$ - $\pi^*$  transitions in the  $sp^2$  dominions of the CDs (bonds C=C and N=C) [47], whereas the latter one arises from  $n$ - $\pi^*$  transitions corresponding to C=O bonds. The absorption spectrum of the WCS molecule (see Scheme 1), shows several absorption bands: one intense band with maximum intensity at 240 nm, a shoulder around 277 nm and a broader and lower intensity band at 395 nm. The CD-WCS spectrum shows an intense band at 254 nm (14 nm red-shifted respect to the 240 nm band of WCS) and a broad band at 365 nm (30 nm blue-shifted respect to the 395 nm band of WCS). However, it is worth noting the presence of absorption side shoulders at 350 nm and 397 nm in the CD-WCS band centred at 365 nm, indicating that this band may be a composite of, at least, two individual components, estimated to be the 350 nm band of CDs and the 395 nm band of WCS, which indicates the successful grafting of WCS on the CDs surface.

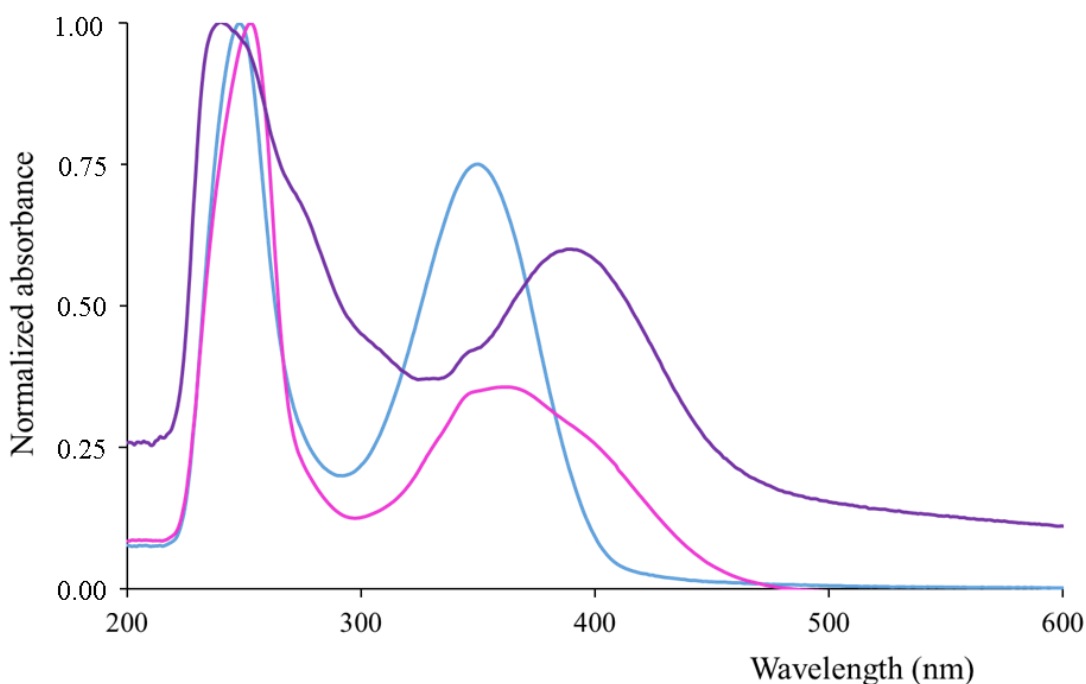


Figure 3. Normalized absorption spectra of WCS (—), CDs (—) and CD-WCS (—)

The photoluminescence spectra of CDs show an excitation band with maximum intensity at 350 nm and an emission band with maximum intensity at 440 nm with mirrored symmetry. A high quantum yield of 49% was calculated, which is consistent with the quantum yield obtained for similar CDs from different sources (Table S2). On the other hand, WCS in water exhibits an excitation band with maximum intensity at 395 nm and an emission band with maximum intensity at 535 nm. CD-WCS, for its part, presents two light emitters (CD and WCS) in the same system. Usually, the close proximity of luminescent systems induces non-radiative energy transfer and extensive intermolecular interactions, thus resulting in emission self-quenching [48]. This effect, however, was not observed in CD-WCS. As seen in Figure 4, upon excitation of CD-WCS at 350 nm (corresponding to the CD excitation maximum), not only the band at 445 nm due to CD emission was observed, but also a band of lower intensity at 535 nm due to WCS emission as result of the partial overlapping of the WCS excitation band with that of the CDs. Neither energy transfer nor spectral shifts were observed in this situation. When the CD-WCS system was excited at 395 nm (corresponding to the WCS excitation maximum), only the emission band due to WCS was observed. A negligible emission shoulder appeared at ca. 440 nm owing to the CDs as result of the marginal overlapping of CD and WCS excitation spectra. Therefore, in this case, no quenching due to aggregation of WCS on the CD surface was observed nor influence of the CD luminescent system on the WCS emission. The luminescent emission of CD-WCS upon the different excitation wavelength can be observed in the inset of Figure 4. When excited at 350 nm (CD excitation maximum) CD-WCS showed a 51% quantum yield (close to that of neat CDs), but only 16% was calculated when excited at 395 nm (absorption maximum of the WCS). Consequently, WCS and CD hold together in the same system (CD-WCS) did not modify/interfere their respective luminescent properties and WCS can act as the signalling moiety for water recognition while the CDs may act as the lubricant additive to improve lubricant tribological properties.

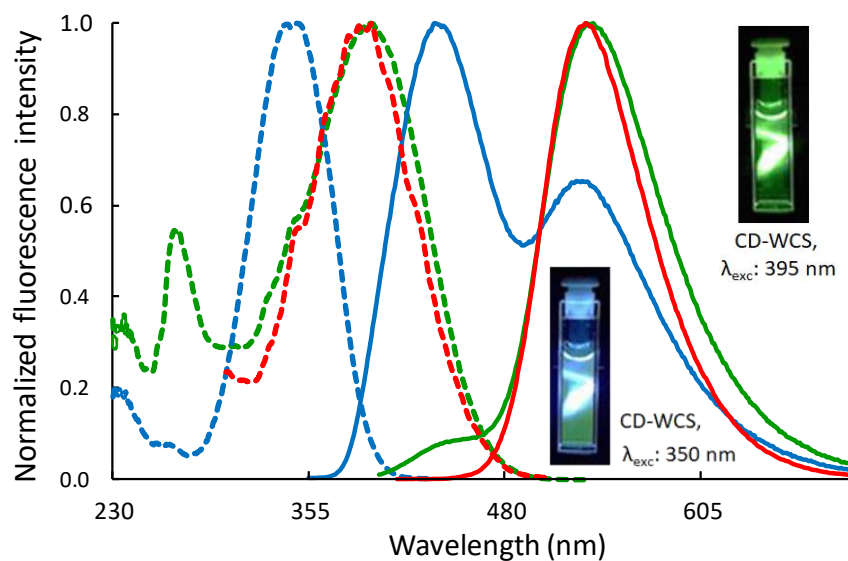


Figure 4. Excitation spectra (dashed lines) and emission (solid lines) of CD-WCS (blue line,  $\lambda_{\text{exc}}$ : 350 nm, green,  $\lambda_{\text{exc}}$ : 395 nm) and WCS (red,  $1 \times 10^{-5}$  M water solution).

#### 4.2.1 Luminescence emission mechanism of the WCS probe in aqueous media.

The rationale behind the luminescence emission of WCS is a photoinduced electron transfer (PET) process. The basic concept relies on the molecular format that includes a three-module “lumophore-spacer-receptor” arrangement, which allows electron transfer from the receptor to the lumophore (or conversely). The PET process and luminescence are competitive processes when the recognition moiety is free but upon binding of the target analyte, the PET process is suspended and luminescence is turned on (Figure 5). In other words, the fluorescence can be switched “off” and “on” by removal or introduction, respectively, of the target analyte.

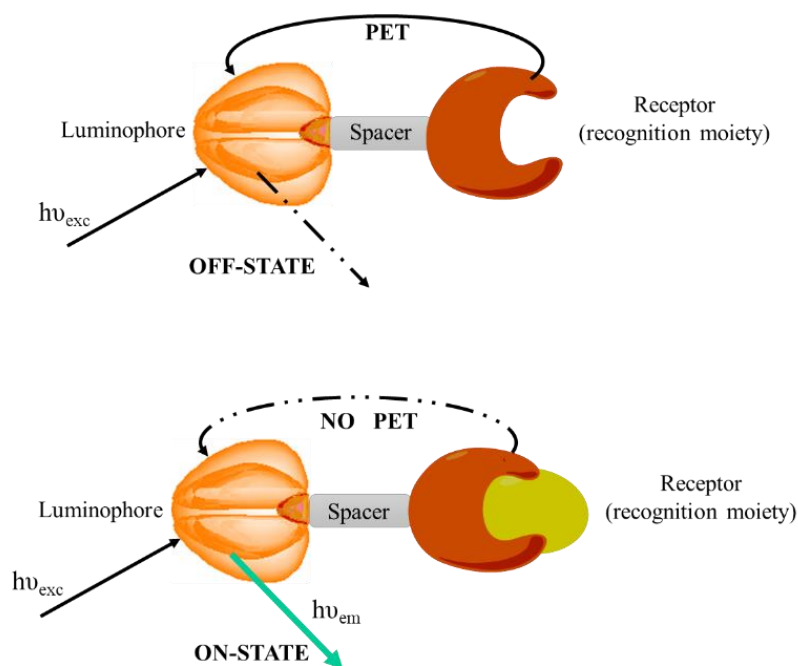


Figure 5. Luminescent PET sensing principle.

In aqueous solution, the structure of the WCS molecule offers the possibility to be used as pH fluorescent PET chemosensor: in the absence of protons the fluorescence of the excited luminophore is quenched by the occurrence of PET processes from the lone pairs of the two amine groups of the piperazine unit to the naphthalimide fluorophore. As the concentration of protons increases, the piperazine amine groups starts to protonate and the fluorescence of the luminophore begins to revive until the original intensity at pH 2. In the intensity versus pH profile in Figure 6, two inflection points at pH 3.10 and 7.45 could be observed, which agreed with the  $pK_{a1}$  (3.81) and  $pK_{a2}$  (8.4) reported for 1,4-disubstituted piperazine [49]. Below pH 4.0, upon protonation of the carboxylic group ( $pK_a \sim 3-4$  for short chain carboxylic acids) [50], the efficiency of the PET process was reduced even more. No other spectral changes but the fluorescence intensity were observed as pH changed in the pH 2-12 range as can be observed in Figure S6. On the other hand, the On-Off process is reversible as it is related to the equilibria between: a) the zwitterionic structure and the di-protonated piperazine ( $pK_a = 3.09$ ) and b) the zwitterionic structure and the non-protonated piperazine ( $pK_a = 7.45$ ), a fact that has been also confirmed in other studies [51]

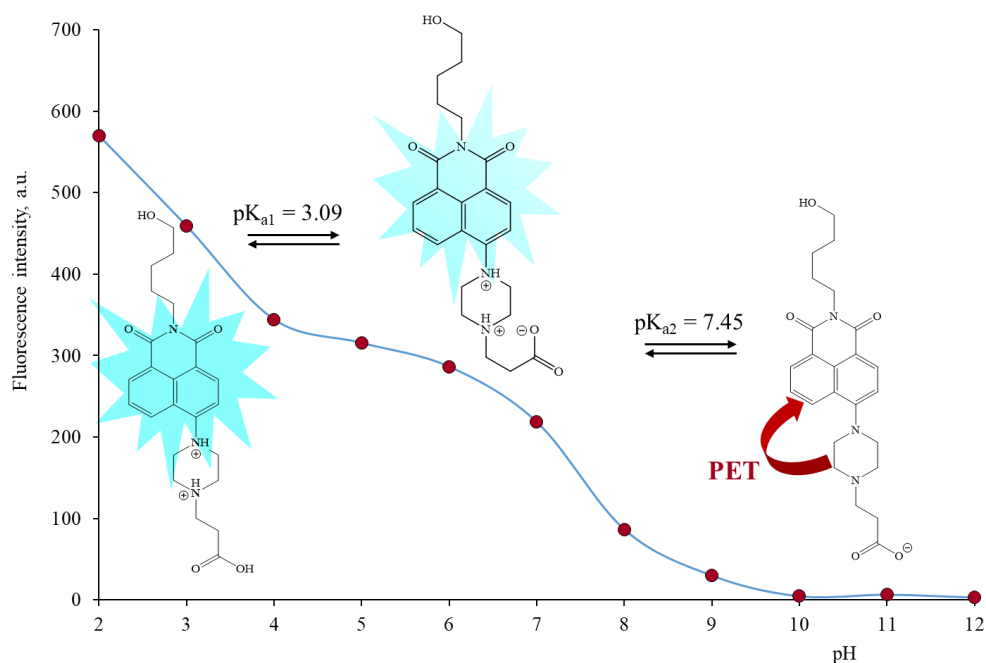


Figure 6. Modulation of the WCS fluorescence intensity (at 530 nm) following protonation of amine and carboxylic groups and proposed PET sensing mechanism ( $\lambda_{exc} = 395$  nm [WCS] =  $1 \times 10^{-5}$  M)

It is interesting to note that in aqueous solution, CD-WCS (WCS immobilized onto the surface of CDs) exhibited the same behaviour that free WCS, what suggests that the immobilization did not modify its capability to recognize  $H^+$  through a PET process similar to the already described one (see Figure S7). Besides its potential as pH chemosensor, we could observe that the fluorescence of WCS also depended on the polarity of the medium, as can be seen in Figure 7 for WCS in different solvents. A considerable red-shift is observed when increasing the solvent polarity, which is ascribed to the solvent reorientation around the excited state of WCS. This results in a reduction of the energy gap between the ground and excited state and thus a decrease of the energy emitted by the molecule.

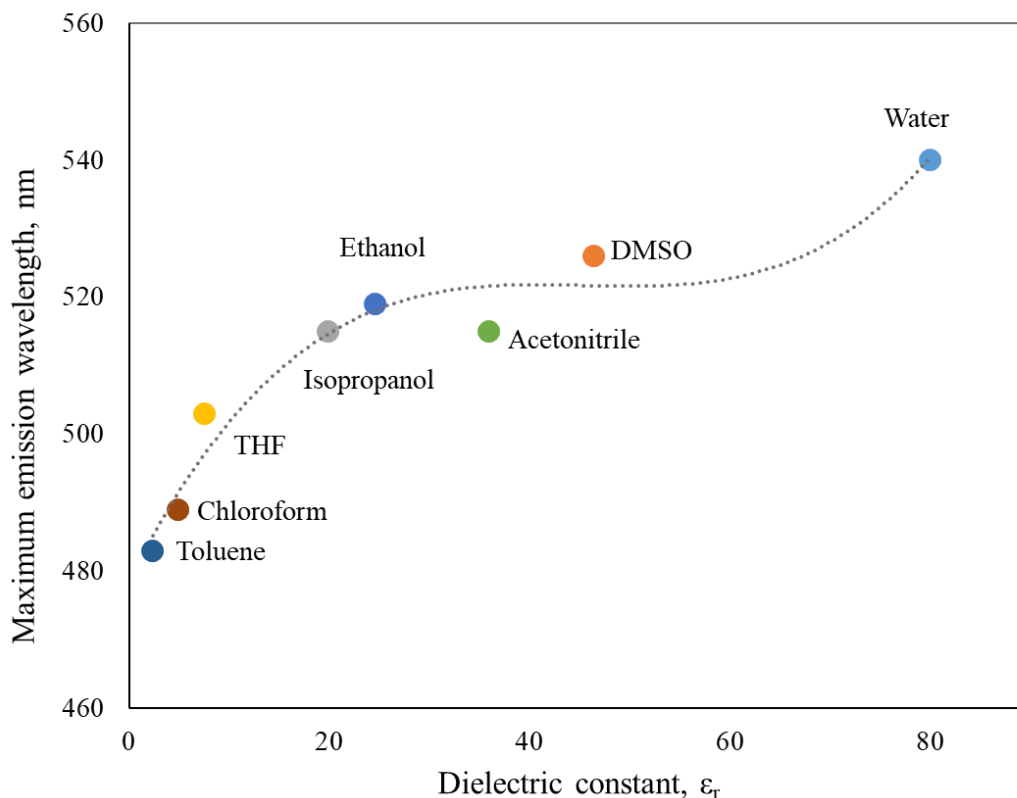


Figure 7. Solvatochromic red shift of WCS versus dielectric constant of the solvent  $\lambda_{exc} = 395$  nm. In all solvents  $[WCS] = 1 \times 10^{-5}$  M.

In a water saturated toluene mixture, free WCS did not exhibit solvatochromism and only a negligible fluorescence intensity change was observed. A possible explanation for this fact, taking into account that water solubility in toluene has been reported to be  $2.66 \times 10^{-2}$  mol.dm<sup>-3</sup> (480 ppm) [52], could be related with the toluene/water interface: H-bond interactions of WCS within interfacial water are less effective than with bulk water owing to an enhancement of the water structure and the H-bond network [53].

#### 4.3. Water quantification in non-aqueous media.

In the light of the solvatochromic behaviour of WCS and with the aim to evaluate the potential of CD-WCS for sensing water in non-aqueous media, we selected toluene as model solvent. We could observe that toluene solutions of CD-WCS exhibited a weak fluorescence at 500 nm when excited at 395 nm (see Figure 8). However, when the water content in the toluene CD-WCS solution was increased, the fluorescence intensity of the CD-WCS also increased in a proportional manner and a weak solvatochromic blue shift (ca. 40 nm) was observed as should be expected due to the lower polarity index of toluene (2.4) compared

to that of water (10.2) [54]. So, as an initial project to test the CD-WCS utility as a fluorimetric sensing material, we tested its recognition behaviour for water contamination in toluene. Taking into consideration the experimental difficulties to work with anhydrous toluene, a commercial toluene with a low water content was used (CT). The concentration of water was, then, determined using the standard addition method as described in the Experimental Section, whose analytical figures of merit are summarized in Table 1. The water concentration in the commercial solvent was found to be  $27 \pm 3$  ppm using the proposed CD-WCS sensing material. The validation of the methodology was carried out by coulometric Karl-Fischer titration (Table 1).

**Table 1.** Analytical performance characteristics of the fluorimetric determination of water in toluene using CD-WCS as sensing material.

Figure of merit	Value		
Calibration line equation	$y = (1.02 \pm 0.03) \cdot 10^3 \cdot x + (28 \pm 3) \cdot 10^3$		
Regression coefficient	0.995		
Linearity (%)	98.9		
Dynamic linear range	DL – 200 ppm (0.02 % v/v)		
Limit of detection (IUPAC)	1.2 ppm (0.00012 % v/v)		
Limit of quantification	4.0 ppm (0.00040 % v/v)		
Relative Standard Deviation	12.3 %		
Validation	Spiked H <sub>2</sub> O, ppm	Found H <sub>2</sub> O, ppm	
		CD-WCS	Karl-Fischer
	0	$27 \pm 3$	$20 \pm 2$
	23	$54 \pm 5$	$43 \pm 4$
	69	$101 \pm 9$	$89 \pm 9$

In Table 1, the content of water using the CD-WCS in toluene showed a strong correlation with those obtained using the Karl-Fischer titration ( $R^2 = 0.9986$ ) (Figure S8). In Figure S9, the spectra of CD-WCS in different pure solvents show a red-shift in the emission maximum from 490 nm in toluene to 502 nm in THF and to 520 nm in ACN, DMSO, isopropanol and ethanol. Trace contamination of these solvents in analytical grade toluene would have a marginal influence on the intensity of the emission maxima of CD-WCS in toluene. So, CD-WCS material could be helpful for rapid and semi-quantitative determination of minor and trace water contamination in low polarity solvents. At this point, we should like to comment that, up to now, only a few modified CDs have been reported as sensing materials for water determination in non-aqueous media (Table 2). In these systems, the detection limits for water determination ranged from 0.01 % v/v using cobalt chloride as CDs modifier [55] in

ethanol to 0.32 % v/v in DMF [56], while data were not validated using an alternative method.

**Table 2.** Recent works on the use of CDs mediated sensing materials for water determination in organic solvents.

CDs starting materials	Sensing mechanism	Solvents	Detection limit, % v/v	Validation	Ref.
o-phenylene-diamine	H bonds, dipole-dipole	Acetone Acetonitrile THF	0.19 0.18 0.13	NO	[26]
Sodium citrate + carbamide + Cobalt chloride	ICT	Ethanol THF 1,4-dioxane	0.01 ---- ----	NO	[55]
Chitosan	PET of PPQ probe	DMSO Ethanol DMF	0.023 0.092 0.32	NO	[56]
Ammonium citrate + amorphous calcium carbonate	Phase transition	Acetonitrile Ethanol THF Acetone	0.0015	NO	[57]
Citric acid + Glutathione	PET of WCS probe	Toluene ISO-32 base oil	0.00012	YES	This work

THF: tetrahydrofuran

ICT: internal charge transfer

DMSO: dimethylsulfoxide

PPQ: 4-(pyridine-2-yl)-3*H*-pirrolo[2,3-*c*]quinoline

PET: photo-electron transfer

Based on these grounds, a more complicated sample, the lubricant base oil ISO-32 gently provided by Repsol, was selected to evaluate the performance of CD-WCS as water chemosensor. Firstly, we explored the intrinsic fluorescent properties of the ISO-32 oil, observing that it showed an intense fluorescence band with maximum intensity at 413 nm when excited at 395 nm. In order to minimize such background fluorescence, oil samples were diluted in CT and a solution of 0.1% v/v ISO-32 oil in CT was used as the sample. In Figure S10a, we can observe that as the water concentration increased the fluorescence intensity at ca. 500 nm due to CD-WCS also increased, which confirms the response of the sensor to the water content in the oil. The standard addition calibration was performed (Figure S10b) and the analytical performance characteristics are collected in Table 3 and a

good correlation between the data provided by the CD-WCS sensing nanomaterial and the Karl-Fischer method (see Figure S8) was obtained.

**Table 3.** Analytical performance characteristics of the fluorimetric determination of water in ISO-32 oil by standard additions method using CD-WCS as sensing material.

Figure of merit	Value	
Calibration line equation	$y = (1.30 \pm 0.04)x + (34 \pm 4)$	
Regression coefficient	0.997	
Linearity (%)	98.9	
Dynamic linear range	Detection limit – 200 ppm (0.02% v/v)	
Limit of detection (IUPAC)	1.4 ppm (0.00014% v/v)	
Limit of quantification	4.7 ppm (0.00047% v/v)	
Relative Standard Deviation	12.7 %	
Water content in ISO-32 oil	CD-WCS	Karl-Fischer
	17±4 ppm	12 ppm

The present CD-WCS may also play a second role as antiwear and antifriction additive in lubricating oils. Our preliminary work on this direction showed that free glutathione CDs showed excellent anti-friction and anti-wear properties when added to a base oil ISO-68 in a 0.5% w/v [1]. A reduction of the friction coefficient of a 36% and a wear reduction of 10% respect to the high viscosity ISO-68 oil were found and these data compared very favourably with those published for CDs used as additives in lubricants of very low viscosity (see additional information and Table S3 in Supplementary Information).

#### 4.4. CD-WCS sensing mechanism in non-aqueous media.

A plausible explanation for the marginal overestimation of water content in non-aqueous media using the CD-WCS probe could be due to the sensing mechanism involved, in which two different phenomena could act simultaneously, so that not only the water content (PET process) but also the polarity of the probe nano-environment (solvatochromism) were measured. The two processes could be summarized as:

- a) In absence of water, the piperazine group plays an essential role, as it behaves as a donor by transfer electrons to the nearby photoexcited naphthalimide moiety, which emission is substantially quenched. On increasing the water content fluorescence is enhanced due to hydrogen bonding interactions established between the piperazine N atoms and water molecules (Figure 8). After these interactions, the lone electron

pairs on the piperazine N atoms are not available for the PET process. Thus, the fluorophore can release the photonic energy in the radiative mode.

b) The fluorescent moiety in CD-WCS is also sensitive to the solvent polarity as we could prove. So, in this particular case, concomitant to the inhibition of the PET process as the water content increased, the polarity of the nano-surroundings was also increasing and a modest reversal (negative) solvatochromism could be observed in the fluorescence spectra (Figure 8). This reversal solvatochromism in the binary mixture toluene-water, in comparison with the free WCS dissolved in dry solvents (Figure 7), could be explained by the blocking of n-electrons in the piperazine moiety through intermolecular H-bonds with water molecules which, in turn, stabilizes the ground state of the probe. The phenomenon of reversal solvatochromism is complex and it has been attributed not only to the solvent polarity but also to dye structural changes, charge transfer processes, interaction of the dye/solvent and hydrogen bonding ability between dye and solvent [58, 59]. Although only Machado's group have reported the first cases of reversal solvatochromism in solvent binary mixtures [60, 61], in our knowledge, this is the first with an analytical application.

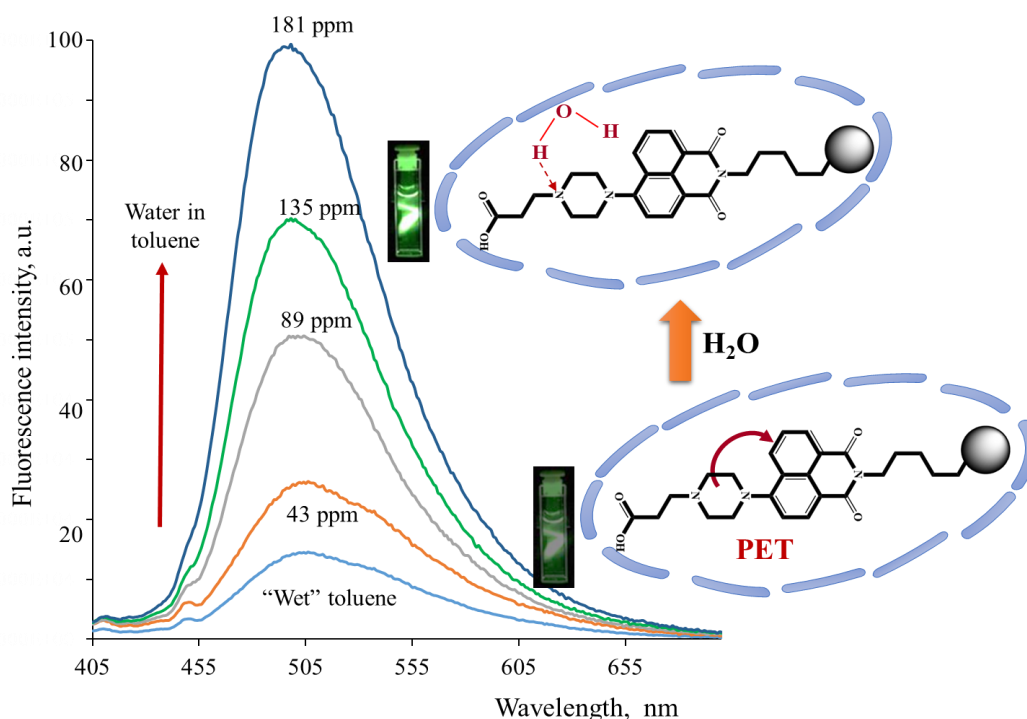


Figure 8. Dependence of the fluorescence emission spectra of CD-WCSs in toluene with water content.  $\lambda_{exc} = 395$  nm. “Wet” toluene (commercial toluene with a water content of 20

ppm determined by the Karl Fischer method). Inset: Proposed PET inhibition-reverse solvatochromic sensing mechanism of CD-WCS

Another question that arises is why the CD-WCS is sensible to the water content in toluene/water mixtures while free WCS doesn't. A reason can be proposed to explain such difference: the presence of the CDs (absent in the free WCS) could be the driving force for the CD-WCS partitions at the water-toluene interface, with the fluorophore immersed in the aqueous phase while the CD could be in contact with both phases due to its solubility in both. It is only a hypothetical picture of the system and further investigations to obtain a comprehensive image of the processes at the water/toluene interface are needed.

## **5. CONCLUDING REMARKS.**

The present paper illustrates the immense possibilities that the PET sensing molecule WCS has not only as chemosensor for  $H^+$  in aqueous media but also once upon bound to CDs (CD-WCS). Besides, due its solubility in non-aqueous media, an advantage of the developed CD-WCS sensing nanomaterial is its sensibility to the solvent polarity. Furthermore, fluorescent CD-WCS chemosensor can be used for the quantitative determination of water contamination in non-aqueous media, such as toluene and lubricant oils. There is an excellent correlation between the water content determined by the CD-WCS sensor and the results obtained by the standard Karl Fischer titration. It is also interesting to note, that most of the CDs described as lubricant additives were used in very low viscosity media (water, polyethylene glycol) while CD-WCS worked in a high viscosity oil, which is a distinct advantage of our system. In this work, emphasis was put on the understanding of the WCS recognition mechanism of  $H^+$  and the CD-WCS signalling mechanism of water contamination in non-aqueous media.

During this study, we noted that the photoluminescence properties (excitation and emission spectra, PET response mechanism) of the fluorescent PET probe was not perturbed by its link to the CD, thanks to the 5-C spacer between the them. Also, we could observe that both free glutathione CDs as well as CD-WCS were highly soluble in the lubricant oil used in this study. An important consequence of these facts is the potential of the CD-WCS to be used also as green additive to bio-based lubricants. It should be emphasized that a wide horizon is open to further investigation and progress is still to be made regarding the applicability of the CD-WCS to simultaneously act as green anti-friction/anti-wear additive and as water contamination sensing probe in complex samples such mineral and biodegradable oils.

## 6. ACKNOWLEDGEMENTS

The authors gratefully acknowledge financial support from the Ministerio de Ciencia, Innovación y Universidades and European Regional Development Fund (MINECO/FEDER), Projects # MAT2015-66747-R\RTI2018-099756-B-I00 and FICYT (Foundation for the Promotion in Asturias of the Applied Scientific Research and Technology), Project FC-GRUPIN-IDI/2018/000131.

- 
- [1] D.B.G. Williams, M. Lawton, *Drying of Organic Solvents: Quantitative Evaluation of the Efficiency of Several Desiccants*, J. Org. Chem. 75, **2010**, 8351-8354. doi.org/10.1021/jo101589h
- [2] R. M. Peltzer, J. Gauss, O. Eisenstein, M. Cascella, *The Grignard Reaction – Unraveling a Chemical Puzzle*, J. Am. Chem. Soc. 142, **2020**, 2984–2994. doi.org/10.1021/jacs.9b11829
- [3] M.F.J. Mabesoone, G.M. ter Huurne, A.R.A. Palmans, E. W. Meijer, *How Water in Aliphatic Solvents Directs the Interference of Chemical Reactivity in a Supramolecular System*, J. Am. Chem. Soc. 142, **2020**, 12400–12408. doi.org/10.1021/jacs.0c04962
- [4] F. Falaki, *Sample preparation techniques for gas chromatography*, Ch.3 in Gas Chromatography-Derivatization, Sample Preparation, Application, Ed. Peter Kusch, IntechOpen, **2019**. doi:10.5772/intechopen.84259
- [5] N.R. Babij, E. O. McCusker, G.T. Whiteker, B. Canturk, N. Choy, L. C. Creemer, C. V. De Amicis, N. M. Hewlett, P.L. Johnson, J. A. Knobelsdorf, F. Li, B. A. Lorsbach, B. M. Nugent, S. J. Ryan, M. R. Smith, Q. Yang, *NMR Chemical Shifts of Trace Impurities: Industrially Preferred Solvents Used in Process and Green Chemistry*, Org. Process Res. Dev. 20, **2016**, 661–667. doi: 10.1021/acs.oprd.5b00417
- [6] Canadian Conservation Institute, “Commercial dry cleaning of museum textiles”, CCI Notes 13/13, 1-2 (2008). <https://www.canada.ca/en/conservation-institute/services/conservation-preservation-publications/canadian-conservation-institute-notes/commercial-dry-cleaning-museum-textiles.html>, last access November 6<sup>th</sup> 2020.
- [7] A. C. Eachus, *The trouble with water*, Tribol. Lubr. Technol., 61, **2005**, 32–38.
- [8] F. Cyriac, P. M. Lugt, R. Bosman, *Impact of Water on the Rheology of Lubricating Greases*, Tribol. Trans., 59, **2016**, 679-689. doi.org/10.1080/10402004.2015.1107929
- [9] R.M. Cresham, G.E. Totten, *Lubrication & Maintenance of Industrial Machinery*; CRC Press: Boca Raton, FL, USA, p. 298, **2009**.

- 
- [10] M. Rauscher, A.J. Tremmel, M. Schardt, A.W.Koch, *Non-Dispersive Infrared Sensor for Online Condition Monitoring of Gearbox Oil*. *Sensors*, 17, **2017**, 399 (2017). doi.org/10.3390/s17020399
- [11] J. Zhu, D. He, E. Bechhoefer; *Survey of Lubrication Oil Condition Monitoring, Diagnostics, and Prognostics Techniques and Systems*; *J. Chem.Sci.Tech.*, 2, **2013**, 100-115.
- [12] N.L.T. Padivitage, J.P. Smuts, D.W. Armstrong; *Water determination* in Specification of Drug Substances and Products. **2014**, Chapter 11, 223-241. <http://dx.doi.org/10.1016/B978-0-08-098350-9.00011-4>
- [13] H.L. Qian, C. Dai, C.X. Yang, X.P. Yan; *High-crystallinity covalent organic framework with dual fluorescence emission and its ratiometric sensing application*; *ACS Appl.Mater.Interfaces*, 2027, 9, 29; <https://doi.org/10.1021/acsami.7b08060>
- [14] C. Chimeno-Trinchet, C. Murru, M.E. Díaz-García, A. Fernández-González, R. Badía-Laíño., *Artificial Intelligence and Fourier-Transform Infrared Spectroscopy for Evaluating Water-mediated Degradation of Lubricant Oils*, *Talanta*, Available online 28 June **2020**, 121312. Doi.16/j.talanta.2020.121312
- [15] Z.Z. Li, C.G. Niu, G.M. Zeng, P.Z. Qin, *Fluorescence Sensor for Water Content in Organic Solvents Based on Covalent Immobilization of Benzothioxanthene*, *Chem Lett.*, 38, **2009**, 698-699. doi: 10.1246/cl.2009.698
- [16] P.Kumar, R. Kaushik, A. Ghosh, D.A. Jose, *Detection of Moisture by Fluorescent OFF-ON Sensor in Organic Solvents and Raw Food Products*, *Anal. Chem.* 88, **2016**, 11314-11318. doi.org/10.1021/acs.analchem.6b03949
- [17] Gao, F., Luo, F., Chen, X. et al, *Fluorometric determination of water in organic solvents using europium ion-based luminescent nanospheres*, *Microchim Acta* 166, **2009**, 163–167. doi.org/10.1007
- [18] Y. Cao, L. Chen, D. Liu, B. Wang, *Multi-responsive red solid emitter: detection of trace water and sense of relative humidity*, *Sci. Chin. Mat.*, 62, **2019**, 823-830. doi.org/10.1007/s40843-018-9371-y
- [19] M. Thuerhong, Y. Xu, X.B. Yin, *Review on Carbon Dots and their Applications*; *Chin. J. Anal. Chem.*, 45, **2017**, 139-150. doi.org/10.1016/S1872-2040(16)60990
- [20] X. Wang, Y. Feng, P. Dong, J. Huang; *A Mini Review on Carbon Quantum Dots: Preparation, Properties, and Electrocatalytic Application*; *Frontiers in Chem.* 7, **2019**, article 671. doi: 10.3389/fchem.2019.00759
- [21] B. Gayen, S. Palchoudhury, J. Chowdhury; *Carbon Dots: A Mystic Star in the World of Nanoscience*; *J. Nanomat.*, **2019**, ID 3451307. doi.org/10.1155/2019/3451307

- 
- [22] M. Semeniuk, Z. Yi, V. Poursorkhabi, J. Tjong, S. Jaffer, Z.H. Lu, M. Sain; *Future Perspectives and Review on Organic Carbon Dots in Electronic Applications*, ACS Nano, 13, **2019**, 6224-6255. doi.org/10.1021/acsnano.9b00688
- [23] Y. Liu, H. Huang, W. Cao, B. Mao, Y. Liu, Z. Kang; *Advances in carbon dots: from the perspective of traditional quantum dots*; Mater.Chem.Front., 4, **2020**, 1586-1613. doi.org/10.1039/D0QM00090F
- [24] J.X. Wu, B. Yan, *A dual-emission probe to detect moisture and water in organic solvents based on green-Tb<sup>3+</sup> post-coordinated metal-organic frameworks with red carbon dots*, Dalton Trans., 46, **2017**, 7098-7105. doi.org/10.1039/C7DT01352C
- [25] J. Wei, Y. Yuan, H. Li, D. Hao, C. Sun, G. Zheng, R. Wang, *A novel fluorescent sensor for water in organic solvents based on dynamic quenching of carbon dots*, New J. Chem., 42, **2018**, 18787-18793. doi: 10.1039/c8nj04365e
- [26] D. Chao, W. Lyu, Y. Liu, L. Zhou, Q. Zhang, R. Deng, M. Zhang, *Solvent-dependent carbon dots and their applications in the detection of water in organic solvents*, J.Mat.Chem.C., 6, **2018**, 7527-7532. doi.org/10.1039/C8TC02184H
- [27] A. Senthamizhan, D. Fragouli, B. Balusamy, B. Patil, M. Palei, S. Sabella, T. Uyar, A. Athanassiou, *Hydrochromic carbon dots as smart sensors for water sensing in organic solvents*, Nanoscale Advances, 1, **2019**, 4258. doi: 10.1039/C9NA00493A
- [28] B. Geng, X. Wang, P. Li, W. Shen, H. Qin, F. Fang, L. Yin, L. Shen, D. Pan, *Multifunctional Carbon Dots for Trace Water Detection, White LEDs, and Bioimaging*, Chemistry Select, 4, **2019**, 14162-14168. doi.org/10.1002/slct.201904133
- [29] <http://spi03.sct.uniovi.es/confocaluniovi/confocaluniovi.htm>
- [30] K. Kanghyeon, L. Wanjin, K.J. Nyoung, K. Hyung Jin, *An off-on fluorescent sensor for detecting a wide range of water content in organic solvents*. Bulletin of the Korean Chemical 34(8), 2013, 2261-2266. doi10.5012/bkcs.2013.34.8.2261
- [31] T. Díaz-Faes López, A. Fernández González, M.E. Díaz-García, R. Badía-Laiño, *Highly efficient Förster resonance energy transfer between carbon nanoparticles and europium-tetracycline complex*. Carbon, 94, **2015**, 142-151. doi.org/10.1016/j.carbon.2015.06.066
- [32] F. Wang, S. Pang, L. Wang, Q. Li, M. Kreiter, C-y. Liu, *One-Step Synthesis of Highly Luminescent Carbon Dots in Noncoordinating Solvents*, Chem. Mater. 22(16), **2010**, 4528-4530. doi.org/10.1021/cm101350u
- [33] J. Zhou, Z. Sheng, H. Han, M. Zou, C. Li, *Facile synthesis of fluorescent carbon dots using watermelon peel as a carbon source*, Mat. Lett 66(1), **2012**, 222-224. doi.org/10.1016/j.matlet.2011.08.081

- 
- [34] Y. Zhuo, H. Miao, D. Zhong, S. Zhu, X. Yang, *One-step synthesis of high quantum-yield and excitation-independent emission carbon dots for cell imaging*, *Mat. Lett.*, 139(15), **2015**, 197-200. doi.org/10.1016/j.matlet.2014.10.048
- [35] K. Dimos, *Carbon Quantum Dots: Surface Passivation and Functionalization*; *Curr. Org. Chem.*, 20, **2016**, 682-695. doi:10.2174/1385272819666150730220948
- [36] K.S. Siow, L. Britcher, S. Kumar, H. J. Griesse, *XPS Study of Sulfur and Phosphorus Compounds with Different Oxidation States*, *Sains Malaysiana* 47(8),**2018**, 1913–1922.doi.org/10.17576/jsm-2018-4708-33
- [37] D. Briggs, D. M. Brewis, R. H. Dahm, I. W. Fletcher, *Analysis of the surface chemistry of oxidized polyethylene: comparison of XPS and ToF-SIMS*. *Surface and Interface Analysis*, 35(2), **2003**,156-167. doi.org/10.1002/sia.1515.
- [38] A.G. Shard, J.D. Whittle, A.J. Beck, P.N. Brookes, N.A. Bullett, R.A. Talib, A. Mistry, D. Barton, S.L. McArthur, *A NEXAFS Examination of Unsaturation in Plasma Polymers of Allylamine and Propylamine*. *J. Phys. Chem. B* 108 (33), **2004**, 12472-12480. doi.org/10.1021/jp048250f
- [39] E. Desimoni, B. Brunetti, *X-Ray Photoelectron Spectroscopic Characterization of Chemically Modified Electrodes Used as Chemical Sensors and Biosensors: A Review*. *Chemosensors* 3(2), **2015**, 70-117. doi.org/10.3390/chemosensors3020070
- [40] H.H. Kyaw, S.H. Al-Harhi, A. Sellai, J. Dutta, *Self-organization of gold nanoparticles on silanated surfaces*. *Beilstein Journal of Nanotechnology*, 6, **2015**, 2345-2353. Doi:10.3762/bjnano.6.242
- [41] R.J.J. Jansen, H. van Bekkum, *XPS of nitrogen-containing functional groups on activated carbon*. *Carbon*, 33(8), **1995**, 1021-1027. doi.org/10.1016/0008-6223(95)00030-H
- [42] T. Das, B.K. Saikia, H.P. Dekaboruah, M. Bordoloi, D. Neog, J.J. Bora, J. Lahkar, B. Narzary, S. Roy, D. Ramaiah, *Blue-fluorescent and biocompatible carbon dots derived from abundant low-quality coals*. *Journal of Photochemistry and Photobiology B: Biology*, 195, **2019**, 1-11. doi.org/10.1016/j.jphotobiol.2019.04.004
- [43] M. Fantauzzi, D. Atzei, *Enargite by XPS*, *Surface Science Spectra* 9, **2002**, 266. doi.org/10.1116/11.20030801
- [44] K.P.C. Vollhardt, N.E. Shore, *Organic Chemistry: Structure and Function*, **2015**, WH Freeman and Company, New York.
- [45] G. Socrates, *Infrared and Raman Characteristic Group Frequencies: Tables and Charts*, John Wiley and Sons, Ltd, Chichester, Third Edition, **2001**.

- 
- [46] L. Lin, S. Zhang, *Creating high yield water soluble luminescent graphene quantum dots via exfoliating and disintegrating carbon nanotubes and graphite flakes*. Chemical Communications, 48(82), **2012**, 10177-10179. doi.org/10.1039/C2CC35559K
- [47] H. Wang, C. Sun, X. Che, Y. Zhang, V.L. Colvin, Q. Rice, J. Seo, S. Feng, S. Wang, W.W. Yu, *Excitation wavelength independent visible color emission of carbon dots*. Nanoscale, 9(5), **2017**, 1909-1915. doi.org/10.1039/C6NR09200D
- [48] J.R. Lakowicz, *Principles of Fluorescence Spectroscopy*, 3rd Ed., Springer, **2006**.
- [49] F. Khalili, A. Henni, A.L.L. East, *pKa Values of Some Piperazines at (298, 303, 313, and 323) K*. Journal of Chemical & Engineering Data, 54(10), **2009**, 2914-2917. doi.org/10.1021/jc900005c
- [50] J.D. Roberts, M.C. Caserio, *Carboxylic acids and their derivatives, in Basic Principles of organic Chemistry*. W. A. Benjamin Inc.: Menlo Park, **1977**.
- [51] Y. Tian, F. Su, W. Weber, V. Nandakumar, B.R. Shuway, Y. Jin, X. Zhou, M.R. Holl, R.H. Johnson, D. R. Meldrum, *A series of naphthalimide derivatives as intra- and extra-cellular pH sensors*, Biomaterials, 31, **2010**, 7411-7422, doi:10.1016/j.biomaterials.2010.06.023
- [52] I. Matsuoka, T. Naito, H. Yamada; *Relationship between the solubility of water in organic solvents and the extraction equilibrium*; Bunseki Kagaku, 51, **2002**, 759-765. doi.org/10.2116/bunsekikagaku.51.759
- [53] S. Strazdaaite, J. Versluis, E.H.G. Backus, H.J. Bakker; *Enhanced ordering of water at hydrophobic surfaces*; J. Chem. Phys., 140, **2014**, 054711. doi: 10.1063/1.4863558
- [54] S. Pedersen-Bjergaard, B. Gammelgaard, T.G. Halvorsen; in *Pharmaceutical Analytical Chemistry*, 2nd Ed. John Wiley & Sons Ltd, **2019**.
- [55] J. Wei, H. Li, Y. Yuan, C. Sun, D. Hao, G. Zheng, R. Wang, *A sensitive fluorescent sensor for the detection of trace water in organic solvents based on carbon quantum dots with yellow fluorescence*; RSC Adv., 8, **2018**, 37028-37034. doi.org/10.1039/C8RA06732E
- [56] S. Pawar, U. K. Togiti, A. Bhattacharya, A. Nag; *Functionalized Chitosan–Carbon Dots: A Fluorescent Probe for Detecting Trace Amount of Water in Organic Solvents*; ACS Omega, 4, **2019**, 11301–11311. doi.org/10.1021/acsomega.9b01208
- [57] H. Yu, H. Li, C. Chen, S. Zhou, P. Wang, *Water-sensitive phase-transition of a carbon dot–calcium carbonate composite for moisture detection in organic solvents*; Anal. Methods, 11, **2019**, 2634-2638. doi.org/10.1039/C9AY00541B

- 
- [58] V. Manzoni, K. Coutinho, S. Canuto; *An insightful approach for understanding solvatochromic reversal*; Chem. Phys. Lett., 655-656, **2016**, 30-34. doi.org/10.1016/j.cplett.2016.05.028
- [59] S. Cha, M.G. Choi, H.R. Jeon, S.K. Chang; *Negative solvatochromism of merocyanine dyes: application as water content probes for organic solvents*; Sensors and Actuators B, 157, **2011**, 14-18. doi:10.1016/j.snb.2011.03.020
- [60] R.O. Stock, A.D.S. Schramm, M.C. Rezende, V.G. Machado; *Reverse solvatochromism in solvent binary mixtures: a case study using a 4-(nitrostyryl)phenolate as a probe*; Phys.Chem.Chem.Phys. 18, **2016**, 202666-20269. doi.org/10.1039/C6CP03875A
- [61] R. I. Stock, C. Sandri, M.C. Rezende, V.G. Machado; *Solvatochromic behaviour of substituted 4-(nitrostyryl)phenolate dyes in pure solvents and in binary solvent mixtures composed of water and alcohols*; J. Mol. Liq.; 264, **2018**, 327-336. doi.org/10.1016/j.molliq.2018.05.042

## SUPPLEMENTARY INFORMATION

### SMART CARBON DOTS AS CHEMOSENSOR FOR CONTROL OF WATER CONTAMINATION IN ORGANIC MEDIA.

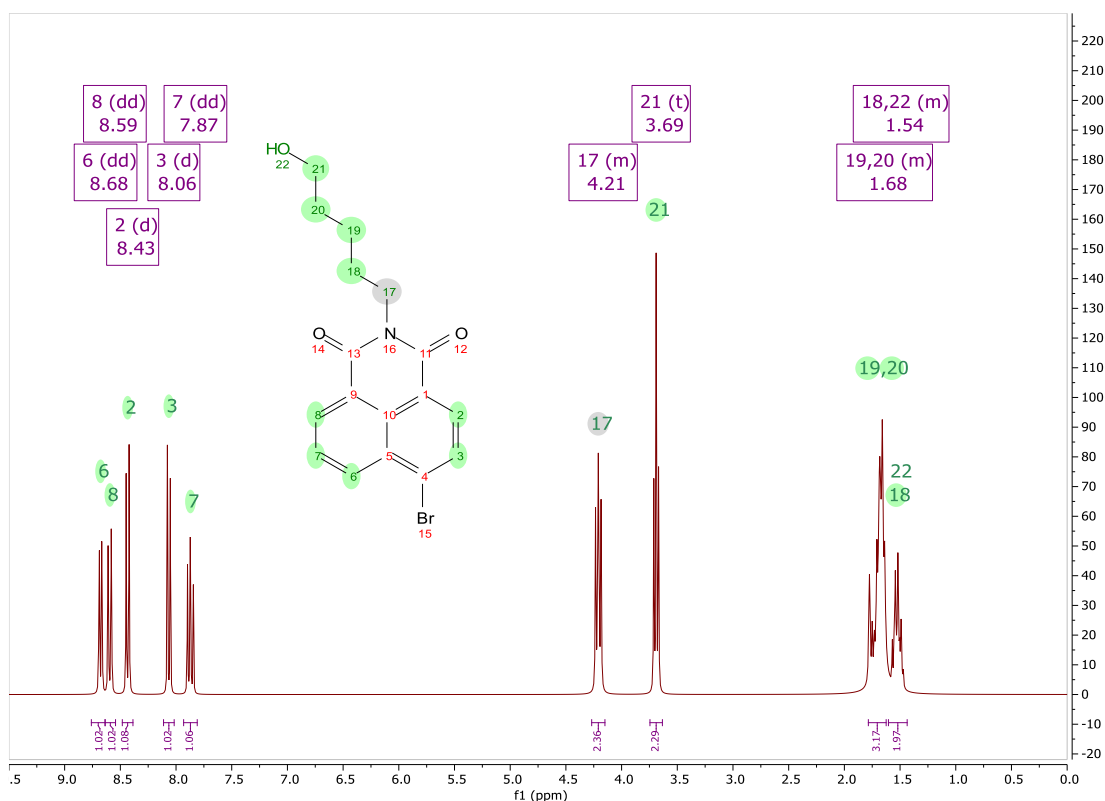
Jorge Espina Casado, Alfonso Fernández-González, Marta E. Díaz-García, Rosana Badía-Laiño

Department of Physical and Analytical Chemistry, University of Oviedo, Oviedo, 33006, Spain.

**Figure S1.**  $^1\text{H}$ -RMN spectra of the different synthesis products.

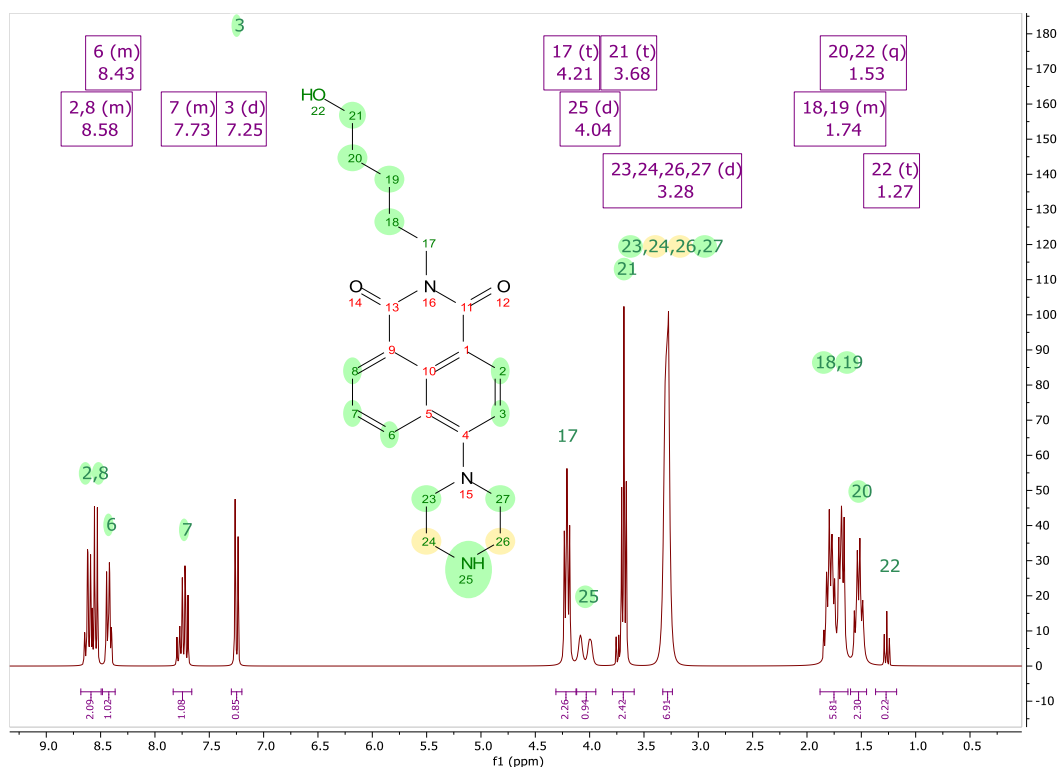
a) 6-bromo-2-(5-hydroxypentyl)-1*H*-benzo[de]isoquinoline-1,3(2*H*)-dione (**P1**):

$^1\text{H}$  NMR (300 MHz, Chloroform-*d*)  $\delta$  8.68 (dd,  $J = 7.3, 1.2$  Hz, 1H), 8.59 (dd,  $J = 8.6, 1.2$  Hz, 1H), 8.43 (d,  $J = 7.9$  Hz, 1H), 8.06 (d,  $J = 7.9$  Hz, 1H), 7.87 (dd,  $J = 8.5, 7.3$  Hz, 1H), 4.27 – 4.15 (m, 2H), 3.69 (t,  $J = 6.4$  Hz, 2H), 1.78 – 1.62 (m, 3H), 1.60 – 1.44 (m, 2H).



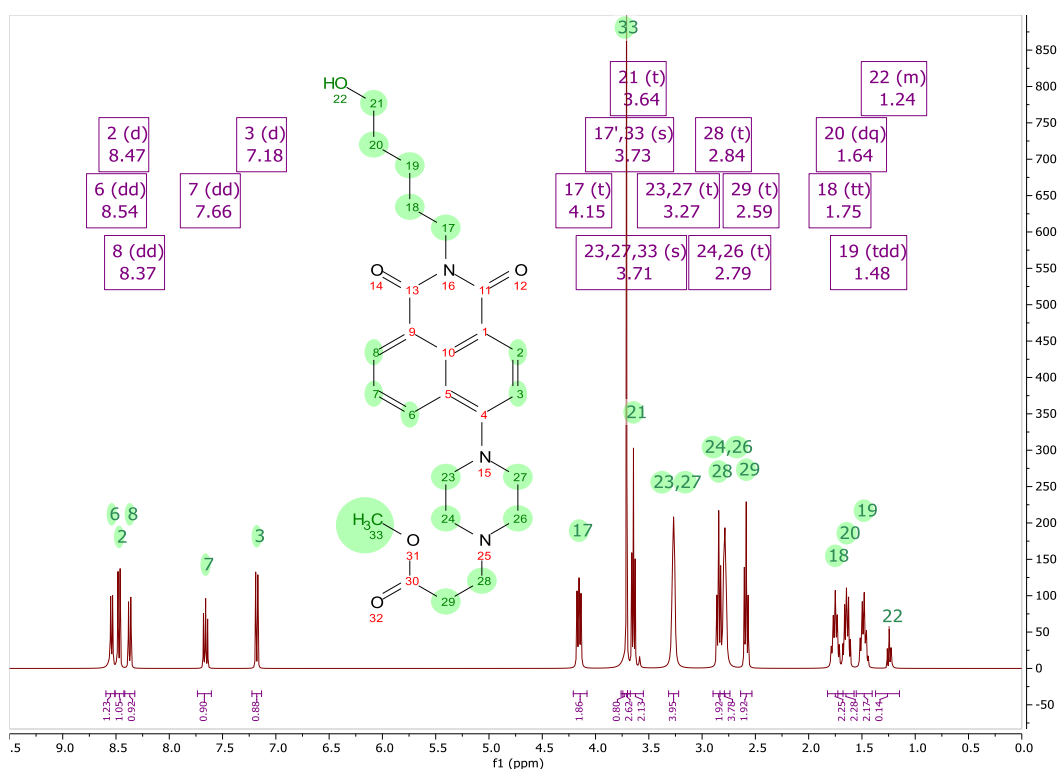
b) 2-(5-hydroxypentyl)-6-(piperazin-1-yl)-1*H*-benzo[de]isoquinoline-1,3(2*H*)-dione (**P2**):

$^1\text{H}$  NMR (300 MHz, Chloroform-*d*)  $\delta$  8.68 – 8.50 (m, 2H), 8.48 – 8.37 (m, 1H), 7.83 – 7.66 (m, 1H), 7.25 (d,  $J = 8.3$  Hz, 1H), 4.21 (t,  $J = 7.4$  Hz, 2H), 4.04 (d,  $J = 27.6$  Hz, 1H), 3.68 (t,  $J = 6.4$  Hz, 2H), 3.28 (d,  $J = 5.8$  Hz, 7H), 1.88 – 1.62 (m, 6H), 1.53 (q,  $J = 8.1$  Hz, 2H).



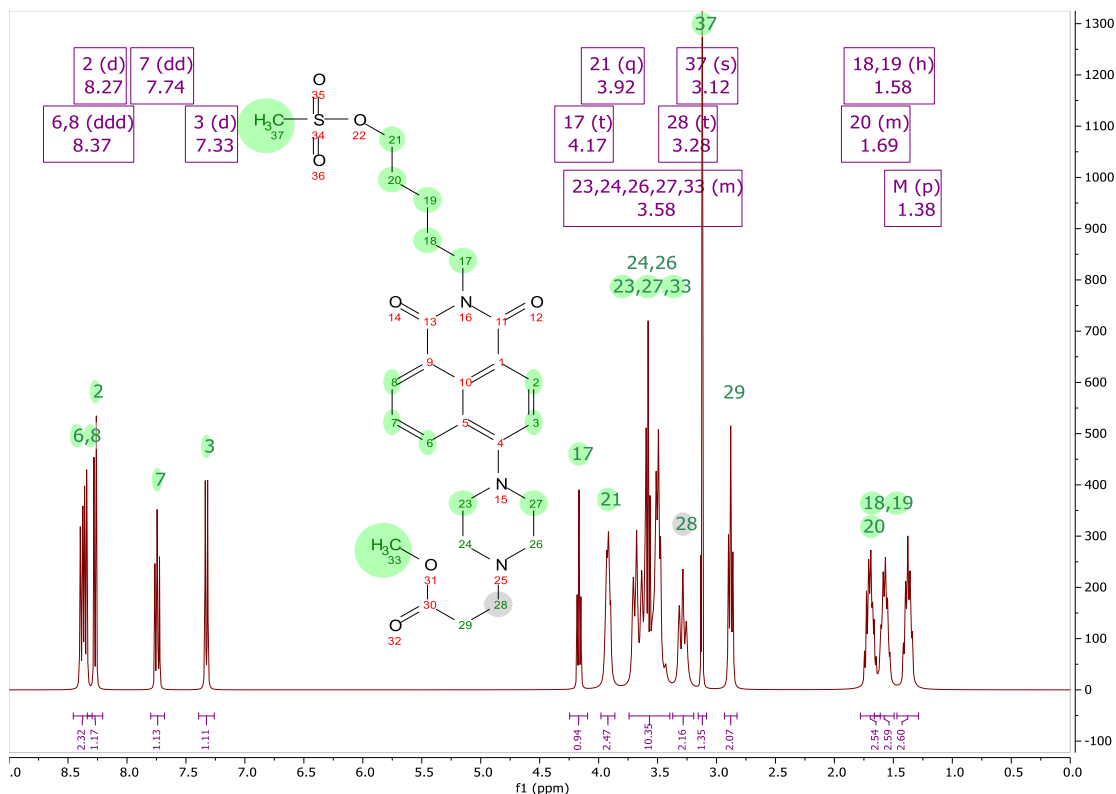
c) Methyl 3-(4-(2-(5-hydroxypentyl)-1,3-dioxo-2,3-dihydro-1*H*-benzo[*de*]isoquinolin-6-yl)piperazin-1-yl)propanoate (**P3**):

<sup>1</sup>H NMR (401 MHz, Chloroform-*d*)  $\delta$  8.54 (dd,  $J = 7.2, 1.2$  Hz, 1H), 8.47 (d,  $J = 8.0$  Hz, 1H), 8.37 (dd,  $J = 8.4, 1.2$  Hz, 1H), 7.66 (dd,  $J = 8.5, 7.3$  Hz, 1H), 7.18 (d,  $J = 8.1$  Hz, 1H), 4.15 (t, 2H), 3.73 (s, 1H), 3.71 (s, 3H), 3.64 (t,  $J = 6.5$  Hz, 2H), 3.27 (t,  $J = 4.8$  Hz, 4H), 2.84 (t,  $J = 7.2$  Hz, 2H), 2.79 (t,  $J = 4.7$  Hz, 4H), 2.59 (t,  $J = 7.2$  Hz, 2H), 1.75 (tt,  $J = 9.0, 6.7$  Hz, 2H), 1.64 (dq,  $J = 8.7, 6.6$  Hz, 2H), 1.48 (tdd,  $J = 9.3, 6.6, 3.5$  Hz, 2H).



d) Methyl 3-(4-(2-(5-((methylsulfonyl)oxy)pentyl)-1,3-dioxo-2,3-dihydro-1*H*-benzo[*de*]isoquinolin-6-yl)piperazin-1-yl)propanoate (**P4**):

$^1\text{H}$  NMR (401 MHz, DMSO-*d*<sub>6</sub>)  $\delta$  8.37 (ddd,  $J = 13.4, 7.9, 1.1$  Hz, 2H), 8.27 (d,  $J = 8.0$  Hz, 1H), 7.74 (dd,  $J = 8.4, 7.3$  Hz, 1H), 7.33 (d,  $J = 8.1$  Hz, 1H), 4.17 (t,  $J = 6.4$  Hz, 1H), 3.92 (q,  $J = 7.4, 6.3$  Hz, 2H), 3.74 – 3.40 (m, 10H), 3.28 (t,  $J = 12.4$  Hz, 2H), 3.12 (s, 1H), 2.88 (t,  $J = 7.5$  Hz, 2H), 1.78 – 1.61 (m, 3H), 1.58 (h,  $J = 7.9$  Hz, 3H), 1.38 (p,  $J = 7.7$  Hz, 3H).



e) 3-(4-(2-(5-hydroxypentyl)-1,3-dioxo-2,3-dihydro-1*H*-benzo[*de*]isoquinolin-6-yl)piperazin-1-yl)propanoic acid (**WCS**):

$^1\text{H}$  NMR (401 MHz, DMSO-*d*<sub>6</sub>)  $\delta$  8.50 – 8.32 (m, 3H), 7.79 (dd,  $J = 8.5, 7.3$  Hz, 1H), 7.31 (d,  $J = 8.1$  Hz, 1H), 4.34 (s, 1H), 4.00 (t,  $J = 7.4$  Hz, 2H), 3.38 (t,  $J = 6.4$  Hz, 2H), 3.22 (t,  $J = 4.5$  Hz, 4H), 2.79 – 2.66 (m, 6H), 2.47 (t,  $J = 7.0$  Hz, 2H), 1.61 (p,  $J = 7.6$  Hz, 2H), 1.52 – 1.40 (m, 2H), 1.40 – 1.26 (m, 2H).

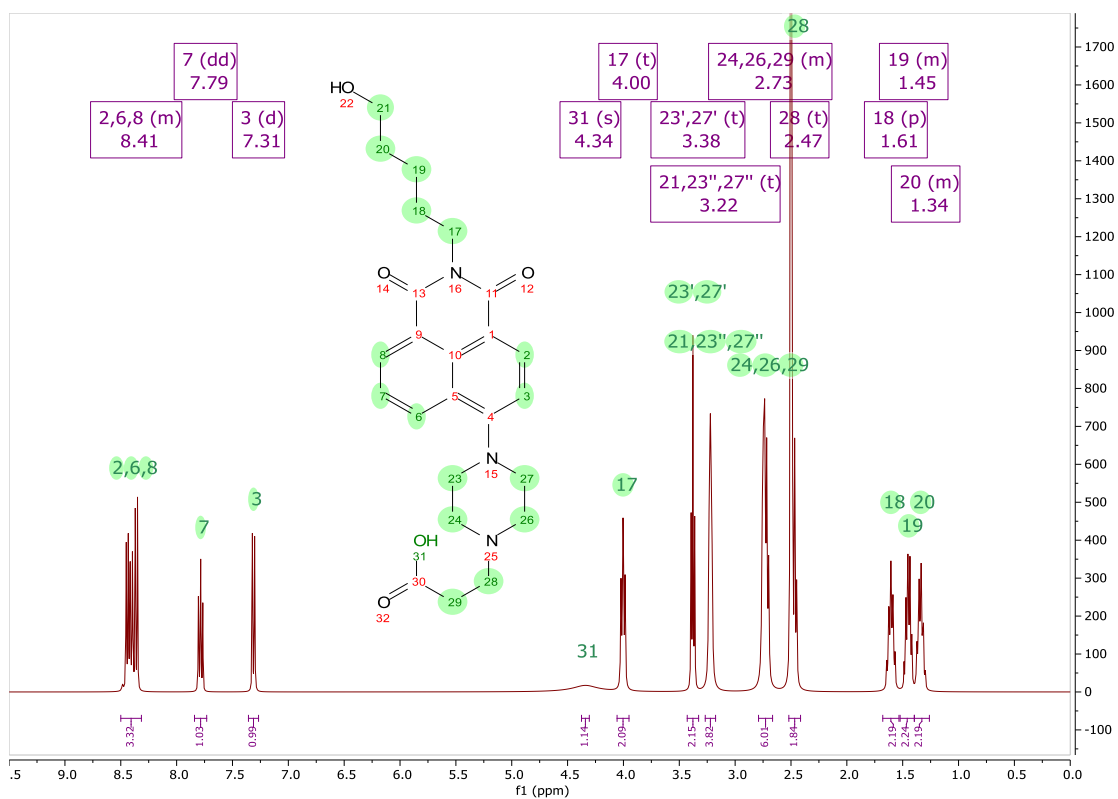
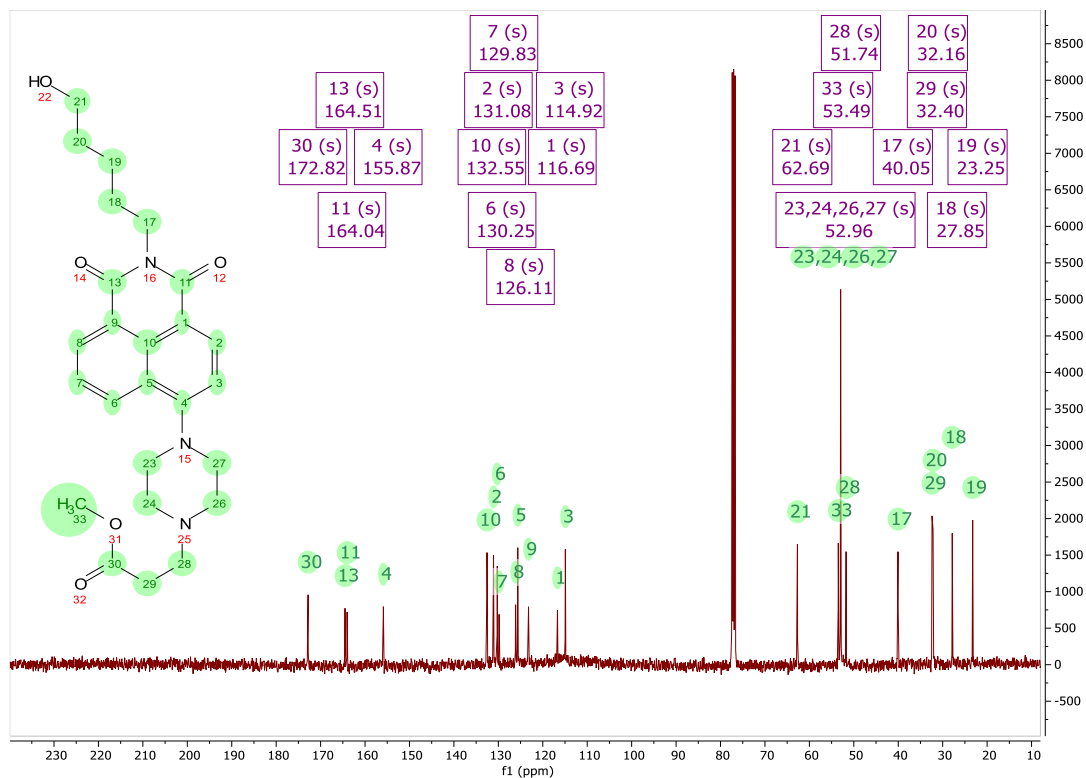


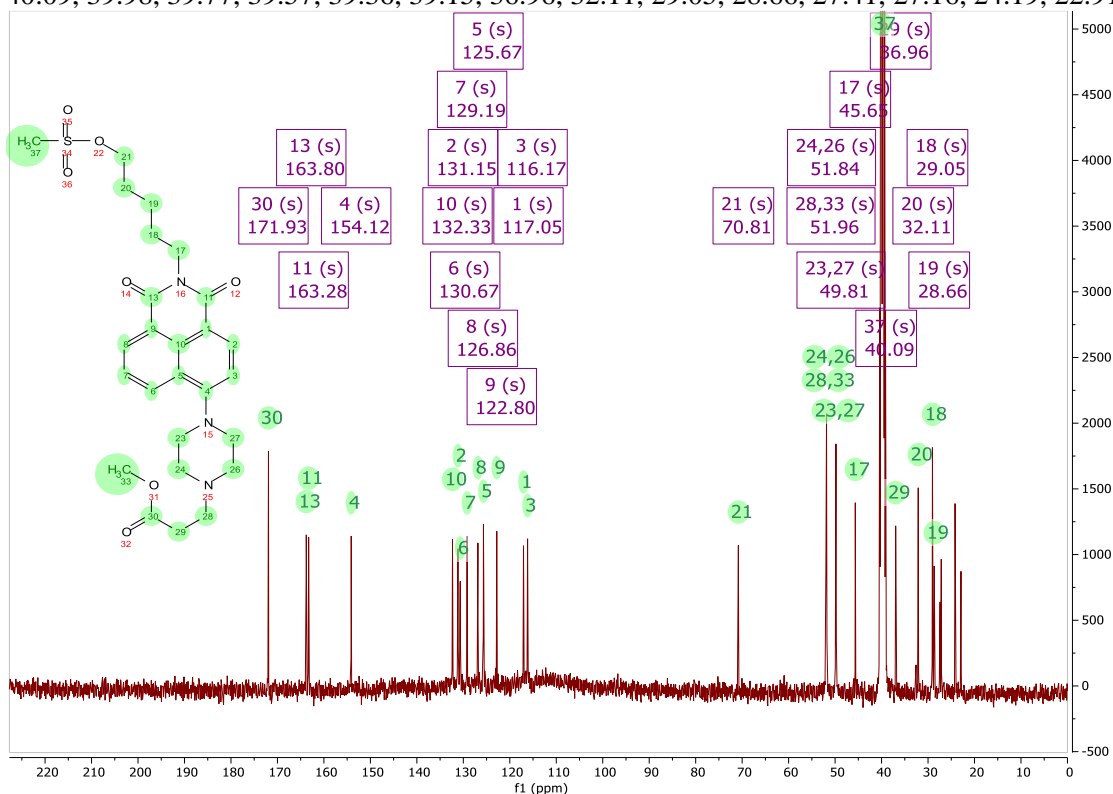
**Figure S2.** <sup>13</sup>C-RMN spectra for synthesis products P3 and WCS.

- a) Methyl 3-(4-(2-(5-hydroxypentyl)-1,3-dioxo-2,3-dihydro-1*H*-benzo[*de*]isoquinolin-6-yl)piperazin-1-yl)propanoate (**P3**):

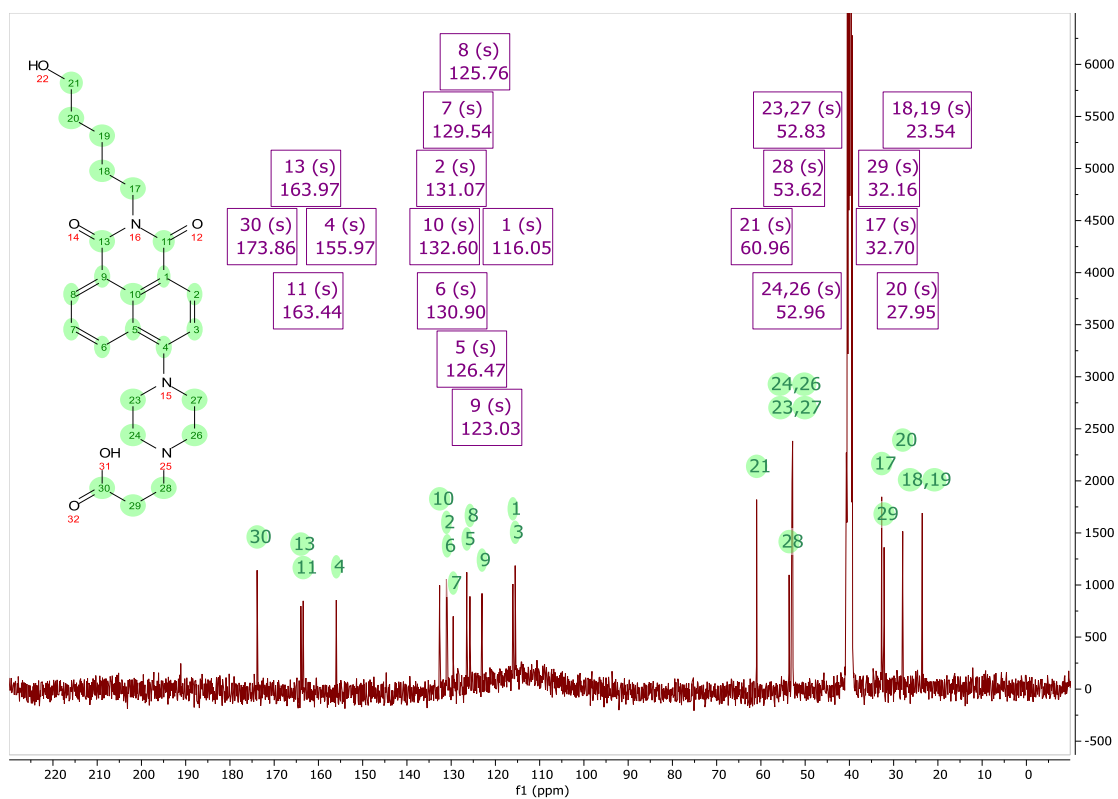
<sup>13</sup>C NMR (101 MHz, CDCl<sub>3</sub>) δ 172.82, 164.51, 164.04, 155.87, 132.55, 131.08, 130.25, 129.83, 126.11, 125.62, 123.21, 116.69, 114.92, 77.36, 77.04, 76.72, 62.69, 53.49, 52.96, 51.74, 40.05, 32.40, 32.16, 27.85, 23.25.



b) Methyl 3-(4-(2-(5-(methylsulfonyl)oxy)pentyl)-1,3-dioxo-2,3-dihydro-1H-benzo[de]isoquinolin-6-yl)piperazin-1-yl)propanoate (**P4**):  
<sup>13</sup>C NMR (101 MHz, DMSO) δ 171.93, 163.80, 163.28, 154.12, 132.33, 131.15, 130.67, 129.19, 126.86, 125.67, 122.80, 117.05, 116.17, 70.81, 51.96, 51.84, 49.81, 45.65, 40.40, 40.19, 40.09, 39.98, 39.77, 39.57, 39.36, 39.15, 36.96, 32.11, 29.05, 28.66, 27.41, 27.16, 24.19, 22.91.



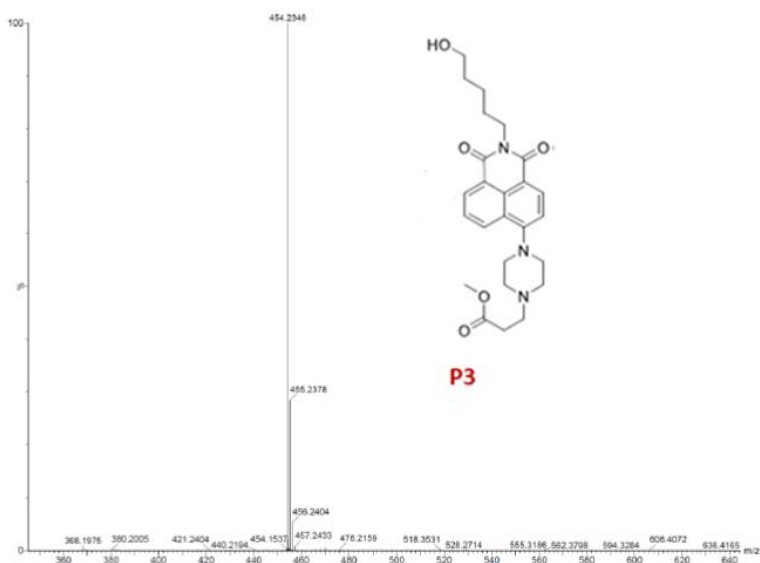
c) 3-(4-(2-(5-hydroxy)pentyl)-1,3-dioxo-2,3-dihydro-1H-benzo[de]isoquinolin-6-yl)piperazin-1-yl)propanoic acid (**WCS**):



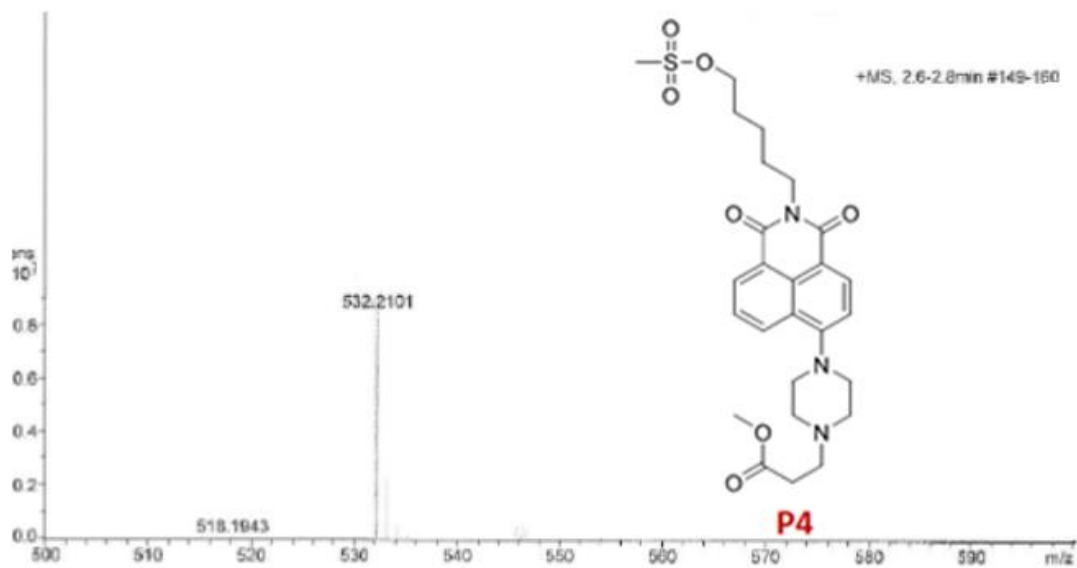
$^{13}\text{C}$  NMR (101 MHz, DMSO)  $\delta$  173.86, 163.97, 163.44, 155.97, 132.60, 131.07, 130.90, 129.54, 126.47, 125.76, 123.03, 116.05, 115.53, 60.96, 53.62, 52.96, 52.83, 40.64, 40.43, 40.22, 40.01, 39.80, 39.59, 39.39, 32.70, 32.16, 27.95, 23.54

**Figure S3.** High-Resolution Mass Spectra of **P3**, **P4** y **WCS** using a positive ionization mode.

- a) Methyl 3-(4-(2-(5-hydroxypentyl)-1,3-dioxo-2,3-dihydro-1*H*-benzo[*de*]isoquinolin-6-yl)piperazin-1-yl)propanoate (**P3**):



- b) Methyl 3-(4-(2-(5-((methylsulfonyl)oxy)pentyl)-1,3-dioxo-2,3-dihydro-1H-benzo[de]isoquinolin-6-yl)piperazin-1-yl)propanoate (**P4**):



- c) 3-(4-(2-(5-hydroxypentyl)-1,3-dioxo-2,3-dihydro-1H-benzo[de]isoquinolin-6-yl)piperazin-1-yl)propanoic acid (**WCS**):

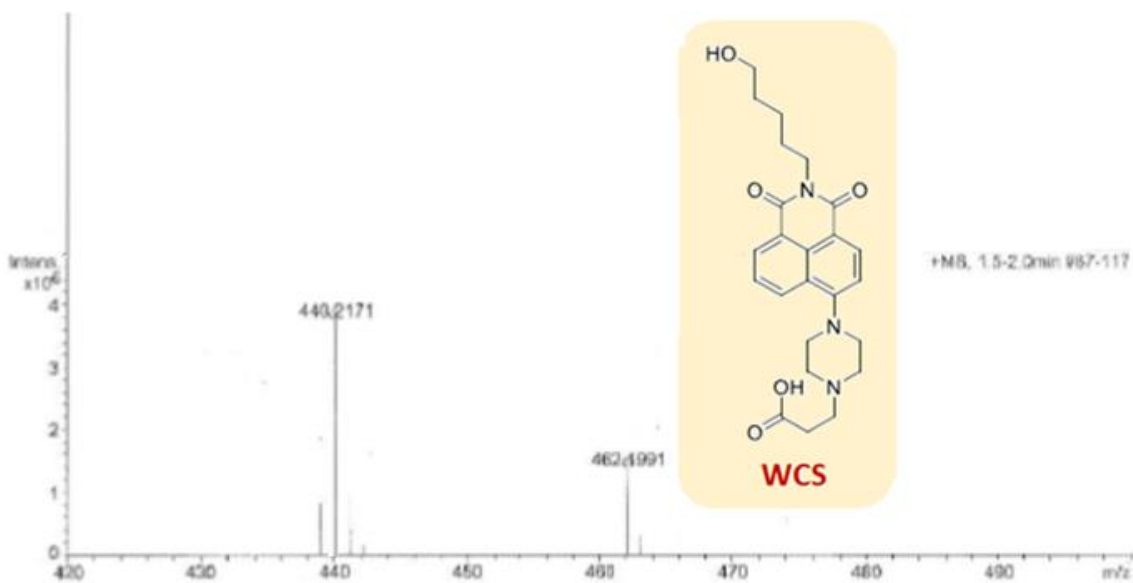


**Figure S4** HR-TEM images of (a) CDs, in which some nanoparticles have been highlighted in circles, (b) interplanar spacing of CDs, (c) CD-WCS, with circles standing out some nanoparticles, (d) interplanar spacing and crystalline orientations present in CD-WCS.

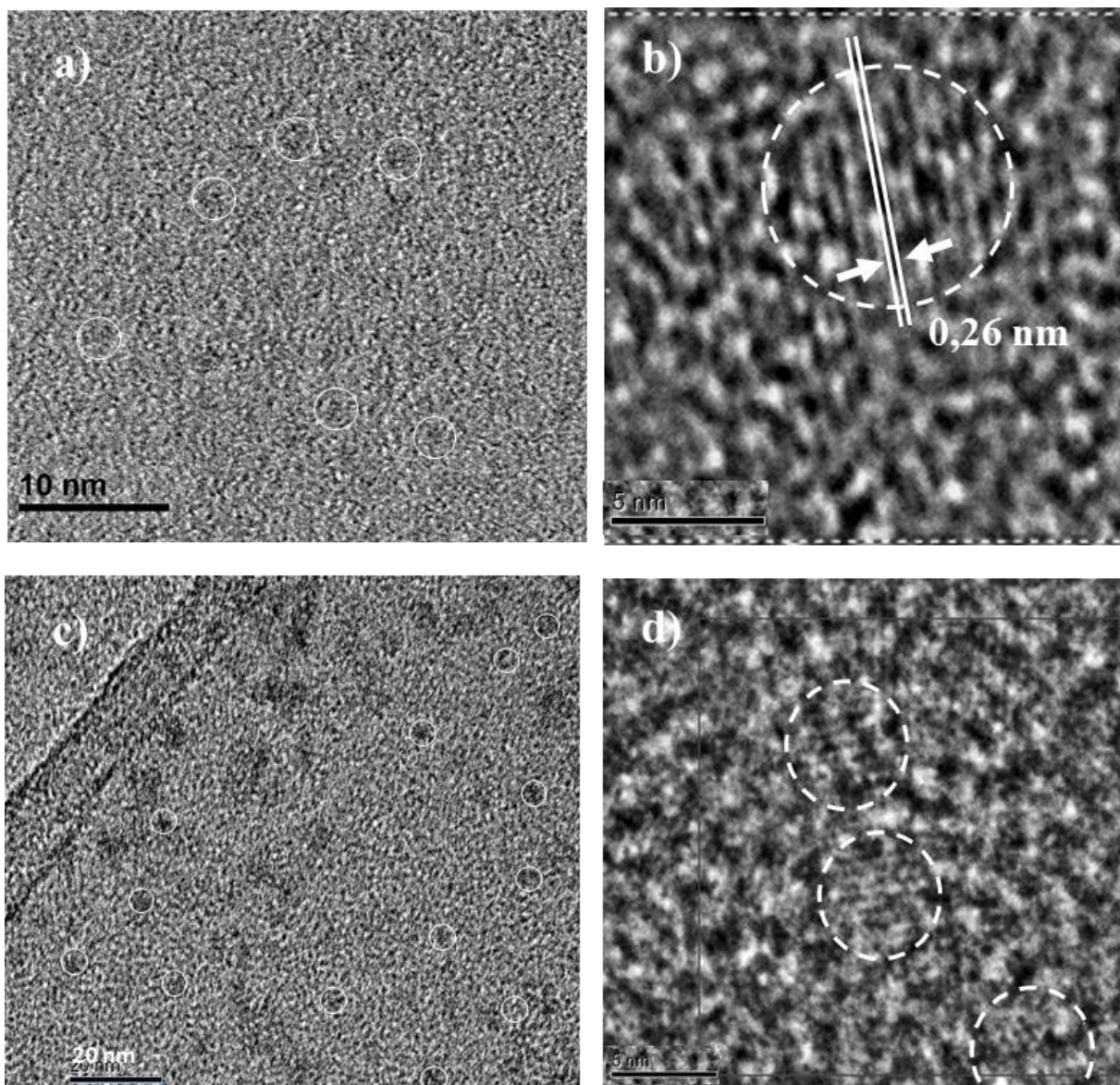


**Figure S5.** Size histograms of a) CDs and b) CDs-WCS based on a random population of 264 nanoparticles, colour envelope showing the normal distribution  $N(\mu, \sigma)$ .

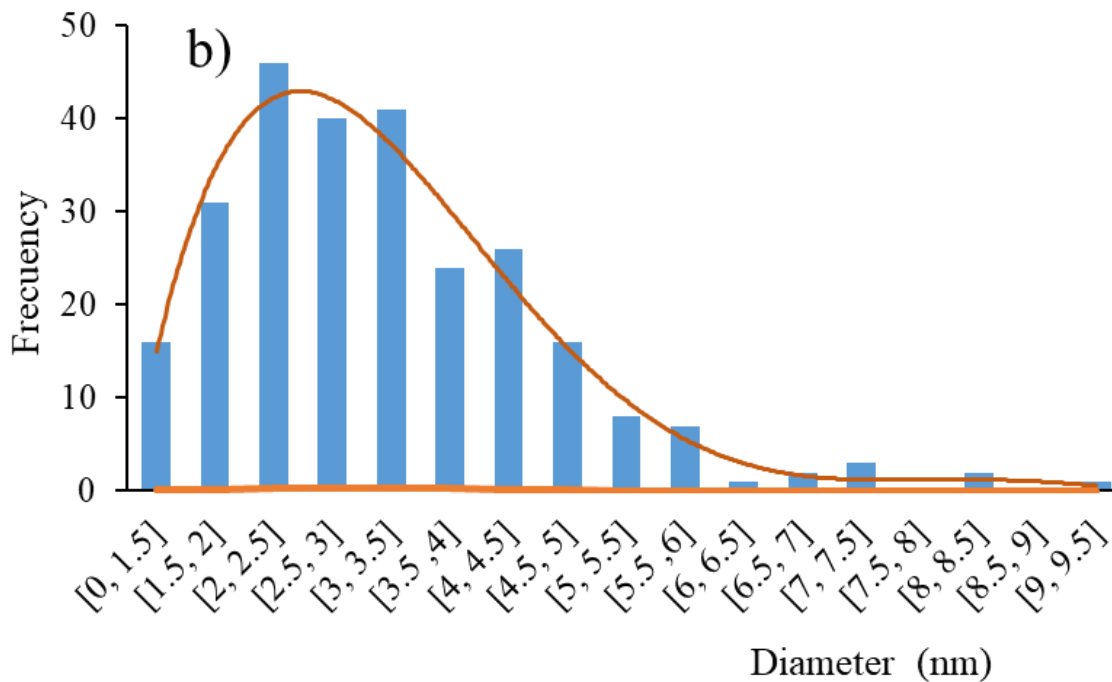
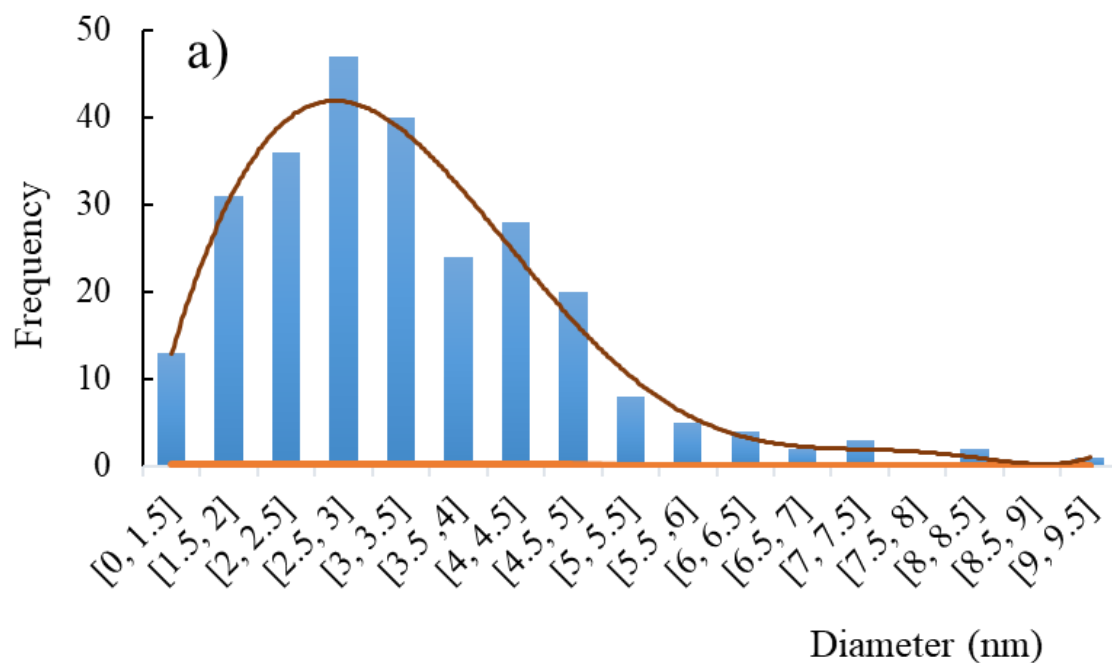


**Figure S6.** Fluorescence emission of free WCS as a function of pH.  $\lambda_{exc} = 395 \text{ nm}$

$[\text{WCS}] = 1 \times 10^{-5} \text{ M}$

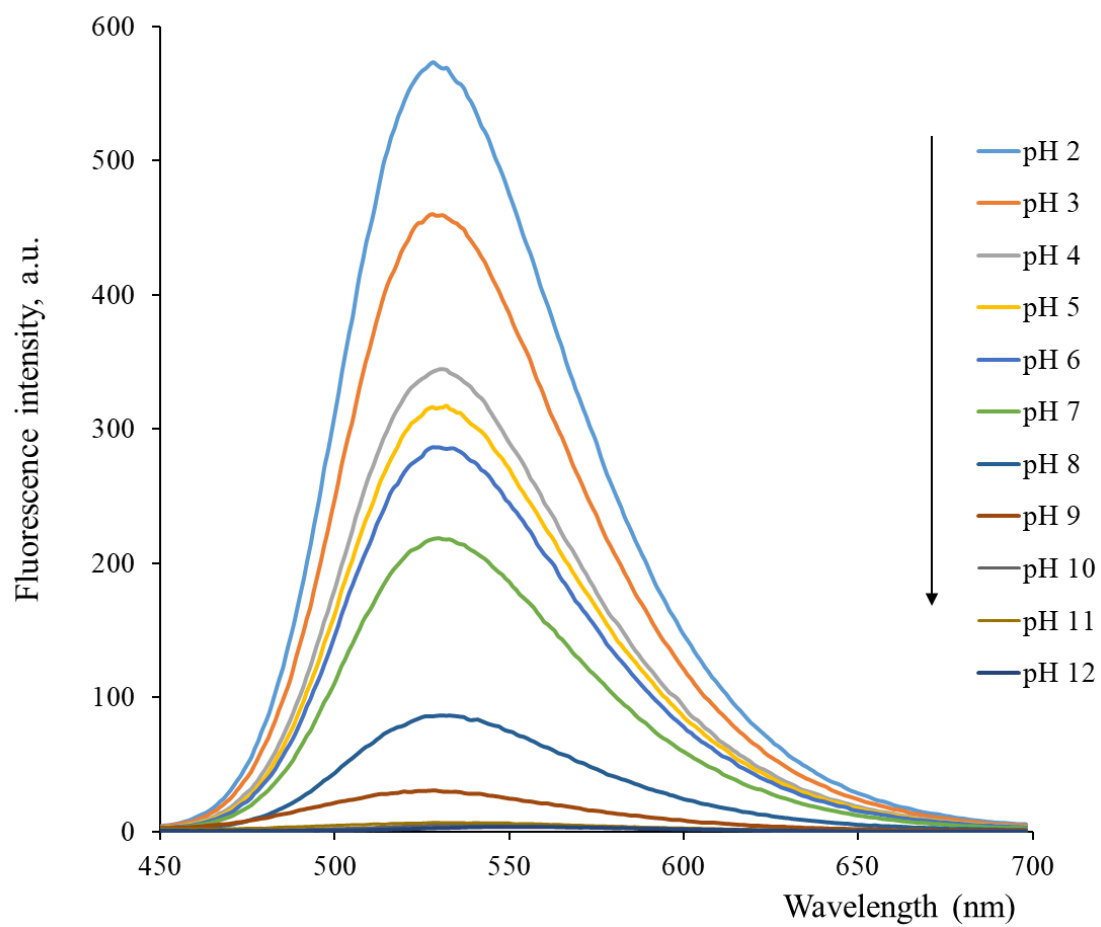


**Figure S7.** Fluorescence emission of CD-WCS as a function of pH.

$\lambda_{\text{exc}} = 345 \text{ nm}$  [CD-WCS] = 1 ppm

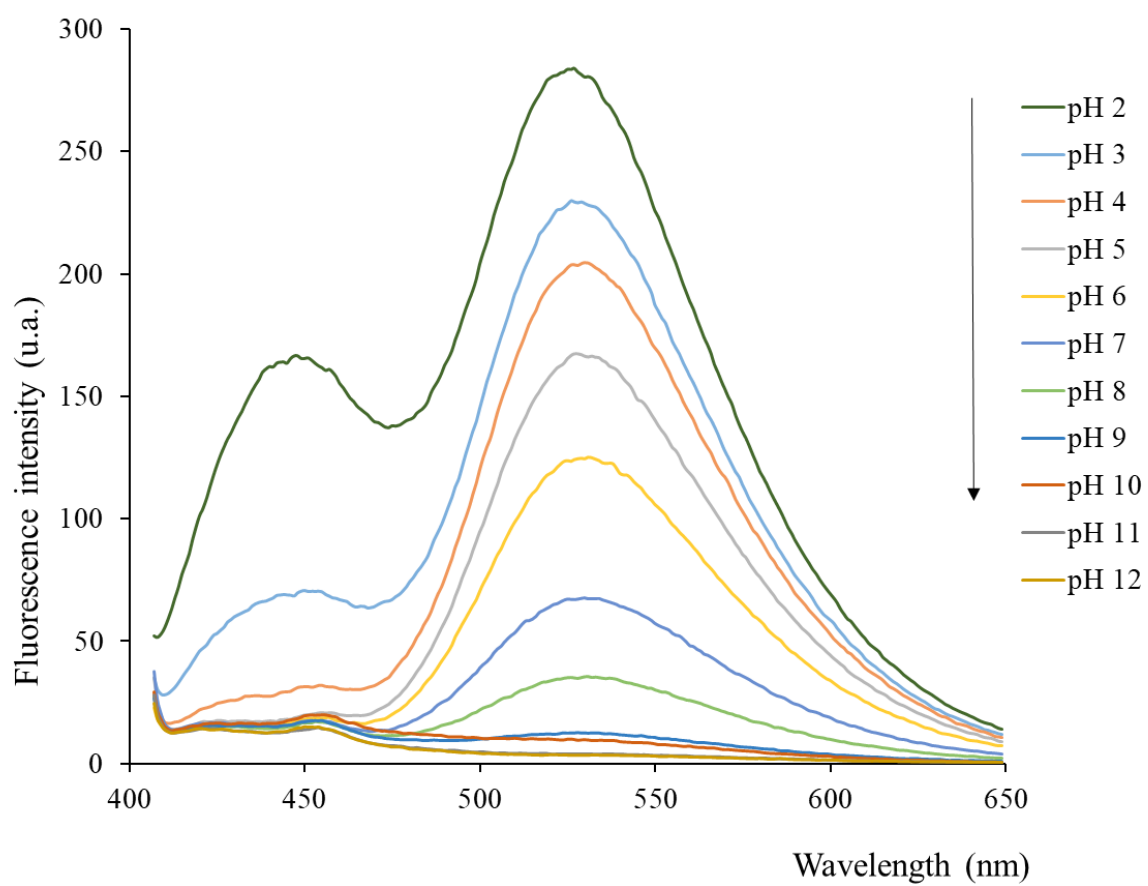


**Figure S8.** Scatter plot showing the correlation between data obtained by the Karl-Fischer method and by the CD-WCS chemosensor.

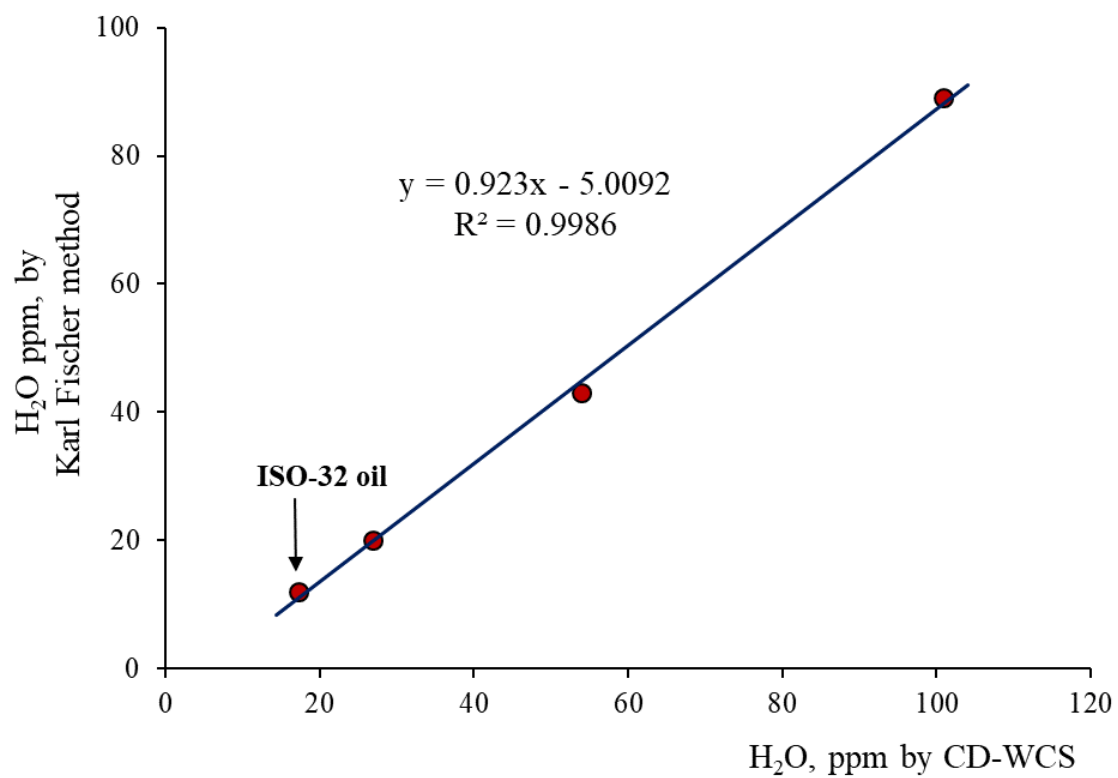


**Figure S9.** Fluorescence spectra of CDs-WCS in different pure solvents. Dotted line indicates the maximum emission of CDs-WCS in toluene and in toluene-water mixtures.

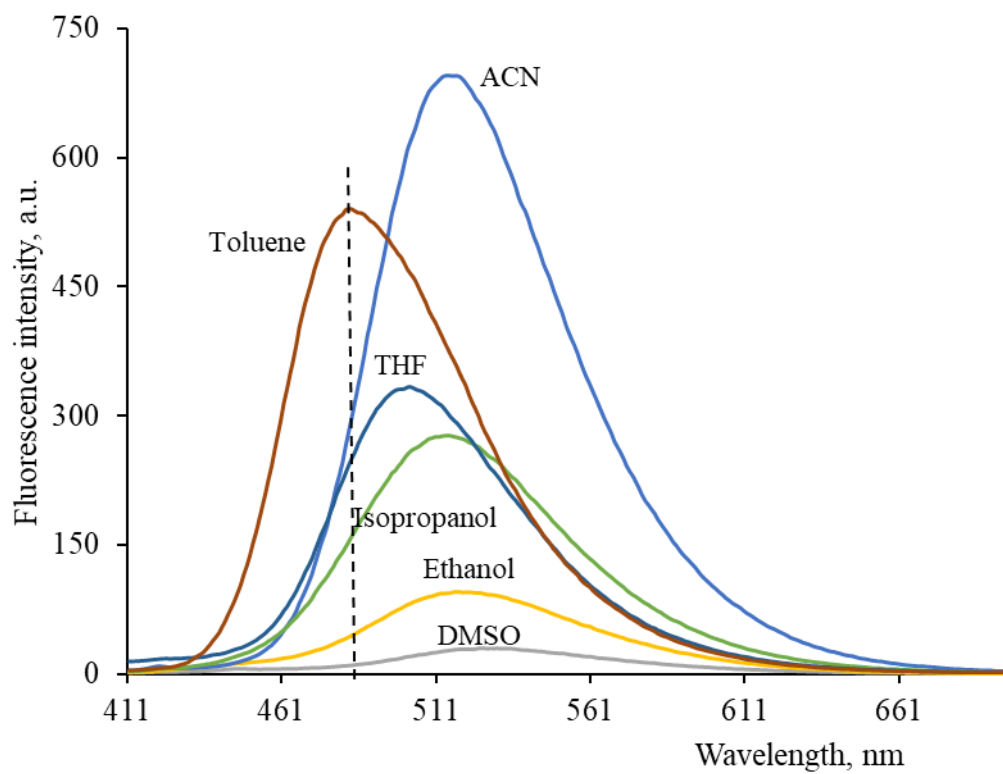


**Figure S10.** (a) Fluorescence emission spectra of base oils solutions ISO-32/toluene 0.1 % v/v without WCS-CDs (blue), and with WCS-CDs (1 ppm) and growing amounts of water. ( $\lambda_{exc}=395$  nm). (b) Calibration line using the standard additions method.

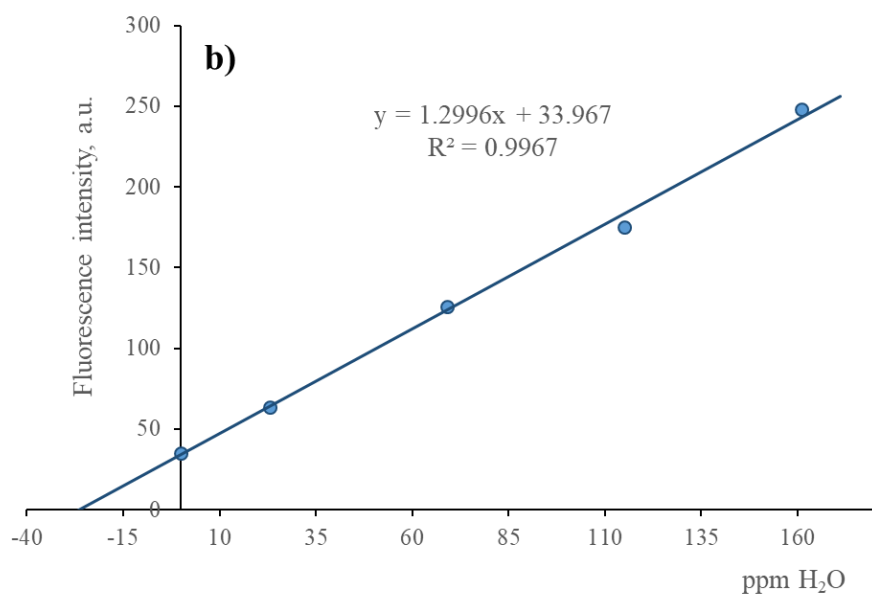
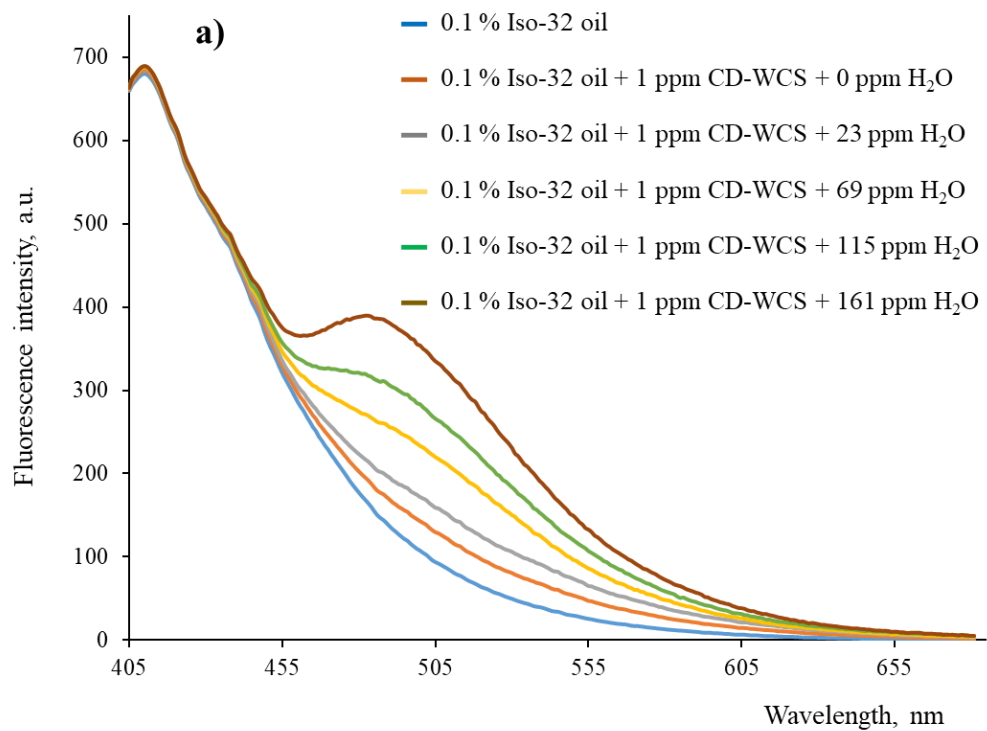


**Table S1.** FTIR bands of the precursor reagents of CDs

	Bands, cm <sup>-1</sup>	Functional Group [1].
Glutathione	3.250	N-H stretching
	2.525	S-H stretching
	1.700	C=O carboxylic group stretching
	1.613, 1.628	In-phase and out-of phase C=O amide stretching vibration
	1.597	N-H scissoring
	1.536, 1.555	N-H bending and C-N stretching in amide group
Citrate	3.452	O-H stretching
	1.595	Asymmetric stretching of C=O (carboxilate)
	1.400	Symmetric stretching of C=O (carboxilate)

**Table S2.** Comparative luminescent quantum yield of carbon dots from different starting materials and synthetic methods.

Carbon quantum dots	Synthesis method	$\Phi$ , Quantum yield (%)	Reference
N-CDs	Hydrothermal	16	[2]
N-GQDs	Hydrothermal	34.5	[3]
C-nanodots	Microwave assisted pyrolysis	30.2	[4]
CQDs	Microwave	10	[5]
GQDs	Pulsed laser ablation	12	[6]
Polydopamine-CDs	Microwave assisted pyrolysis	5	[7]
Chitosan-CDs	Carbonization	4.34	[8]
CDs	Hydrothermal	49	This work

GQDs: Graphene quantum dots

**Table S3.** Comparison of tribological performance characteristics of CDs from different sources

CD precursors	Lubricant Viscosity (cSt)	Friction coefficient	Wear	Concentration w/v, %	Ref.
Sodium citrate + sodium thiosulphate	Water 1	-30%	-58%	1,25	[9]
BSA	Water 1	+25%	+600%	N.P.	[10]
Citric acid + 4-amine-diphenylamine	PEG 200 4,4	-75%	-42%	1	[11]

Citric acid + [AmIm][Br]	PEG 200 4,4	-70%	-33%	0,3	[12]
Citric acid+ ethylene- diamine + nickel acetate	PEG 200 4,4	-35,5	-36,4	2,0	[13]
Citric acid + glutathione	Oil ISO 68 68	-36%	-10%	0,5	This work

BSA: Bovine serum albumin

N.P. Not provided

PEG: poly-ethylene-glycol

[AmIm][Br]: ionic liquid 1-aminopropyl-3-methyl-imidazolium bromide

### Tribological characterization test

In this work, the tribological characterization of the glutathione carbon dots (CDs) as lubricant additives was evaluated using suspensions of the CDs in base oil ISO-68 with concentrations of 0.1%, 0.25% and 0.5% w/v. Samples were sonicated for 15 minutes in order to improve the dispersion process. The tribological assay was carried out employing 4.5 mL of CD lubricating suspension in a tribometer BRUKER UMT 3 with a reciprocating ball-on-plate configuration, with upper chrome plated steel AISI 52100 balls (9.5 mm diameter, 63 HRC hardness, <0.05  $\mu\text{m}$  of surface finish (Ra). The lower AISI 52100 steel disks (190-210 HV30 hardness, < 0,02  $\mu\text{m}$  of surface finish (Ra). 20-min tests were performed under a normal load of 60N (corresponding to an average Hertzian contact pressure of 1.6 Gpa), with a stroke length of 4 mm and 15 Hz of reciprocating frequency. Wear scar of the disks was measured using a confocal microscope. At least, three tests were performed for every CD lubricating suspension. To ensure repeatability, new balls and disks were used for each test. Prior to testing, all components were cleaned with heptane using ultrasound for 5 minutes, rinsed with ethanol and air dried.

---

### REFERENCES

- [1] G. Socrates, *Infrared and Raman Characteristic Group Frequencies: Tables and Charts*, John Wiley and Sons, Ltd, Chichester, Third Edition, **2001**.
- [2] Z. Liang, L. Zeng, X. Cao, Q. Wang, X. Wang, R. Sunab, *Sustainable carbon quantum dots from forestry and agricultural biomass with amplified photoluminescence by simple NH<sub>4</sub>OH passivation*. *Journal of Materials Chemistry C*, 2(45), **2014**, 9760-9766. doi: org/10.1039/C4TC01714E

- 
- [3] Y. Dai, H. Long, X. Wang, Y. Wang, Q. Gu, W. Jiang, Y. Wang, C. Li, T. H. Zeng, Y. Sun, J. Zeng, *Versatile Graphene Quantum Dots with Tunable Nitrogen Doping*. *Particle & Particle Systems Characterization*, 31(5), **2014**, 597-604. doi: org/10.1002/ppsc.201300268
- [4] X. Zhai, P. Zhang, C. Liu, T. Bai, W. Li, L. Daic, W. Liu, *Highly luminescent carbon nanodots by microwave-assisted pyrolysis*. *Chemical Communications*, 48(64), **2012**, 7955-7957. doi: org/10.1039/C2CC33869F
- [5] Y.F. Huang, X. Zhou, R. Zhou, H. Zhang, K.B. Kang, M. Zhao, Y. Peng, Q. Wang, H.L. Zhang, W.Y. Qiu, *One-Pot Synthesis of Highly Luminescent Carbon Quantum Dots and Their Nontoxic Ingestion by Zebrafish for In Vivo Imaging*. *Chemistry – A European Journal*, 20(19), **2014**, 5640-5648. doi: 10.1002/chem.201400011
- [6] T. N. Lin, K. H. Chih, C. T. Yuan, J. L. Shen, C. A. J. Lince, W. R. Liu, *Laser-ablation production of graphene oxide nanostructures: from ribbons to quantum dots*. *Nanoscale*, 7(6), **2015**, 2708-2715. doi: org/10.1039/C4NR05737F
- [7] Y. Bai, B. Zhang, L. Chen, Z. Lin, X. Zhang, D. Ge, W. Shi, Y. Sun, *Facile One-Pot Synthesis of Polydopamine Carbon Dots for Photothermal Therapy*. *Nanoscale research letters*, **13**(1), **2018**, 287-287. doi: 10.1186/s11671-018-2711-2
- [8] X. Liu, J. Pang, F. Xu, X. Zhang, *Simple Approach to Synthesize Amino-Functionalized Carbon Dots by Carbonization of Chitosan*. *Scientific Reports*, 6, **2016**, 31100. doi: 10.1038/srep31100
- [9] H.P. Xiao, S.H. Liu, Q. Xu, H. Zhang, *Carbon quantum dots: An innovative additive for water lubrication*, *Science China Technological Sciences*, 62(4), **2019**, 587-596. doi.org/10.1007/s11431-018-9330-y
- [10] A.M. Tomala, V.B. Kumar, Z. Porat, R. Michalczewski, A. Gedanken, *Tribological anti-wear and extreme-pressure performance of multifunctional metal and nonmetal doped C-based nanodots*, *Lubricants*, 7(4), **2019**, 36. doi.org/10.3390/lubricants7040036
- [11] M. Ye, T. Cai, W. Shang, L. Zhao, Y. Zhang, D. Liu, S. Liu, *Friction-induced transfer of carbon quantum dots on the interface: Microscopic and spectroscopic studies on the role of inorganic-organic hybrid nanoparticles as multifunctional additive for enhanced lubrication*, *Tribology International* 127, **2018**, 557-567. doi.org/10.1016/j.triboint.2018.06.033
- [12] B. Wang, W. Tang, H. Lu, Z. Huang, *Ionic liquid capped carbon dots as a high-performance friction-reducing and antiwear additive for poly(ethylene glycol)*, *Journal of Materials Chemistry A*, 4(19), **2016**, 7257-7265. doi.org/10.1039/C6TA01098A
- [13] Z. Tu, E. Hu, B. Wang, K.D. David, P. Seeger, M. Moneke, R. Stengler, K. Hu, X. Hu *Tribological behaviors of Ni-modified citric acid carbon quantum dot particles as a green additive in polyethylene glycol*, *Friction*, 8, **2020**, 182–197. doi.org/10.1007/s40544-019-0272-8